Multiple knockout mouse and embryonic stem cell models reveal the role of *miR-124a* in neuronal maturation

多重欠損のマウスと ES 細胞モデルにより明らかとなった *miR-124a* の神経成熟における役割

大阪大学 理学研究科 生物科学専攻

分子発生学研究室

(PI: 古川 貴久 教授)

前田 和

Abstract

MicroRNAs (miRNAs) are small non-coding RNA molecules that regulate the gene expression of various biological processes in plants and animals. A large number of miRNAs are expressed in the vertebrate central nervous system (CNS). *MicroRNA-124a* (*miR-124a*) is one of the most abundantly expressed miRNAs in the CNS. The nucleotide sequence of *miR-124a* and its nervous system-specific expression pattern are evolutionarily highly conserved from *Caenorhabditis elegans* (*C. elegans*) to all studied vertebrates, including human. *miR-124as* are encoded in mammals by the three genomic loci *miR-124a-1/2/3*; however, its *in vivo* roles in neuronal development and function remain ambiguous.

In the present study, we investigated the effect of *miR-124a* loss on neuronal differentiation in mice and in embryonic stem (ES) cells by generating and analyzing multiple knockout models. Since *miR-124a-3* exhibits only background expression levels in the brain and we were unable to obtain *miR-124a-1/2/3* triple knockout (TKO) mice by mating, we generated and analyzed *miR-124a-1/2* double knockout (DKO) mice. We found that these DKO mice exhibit perinatal lethality. RNA-sequencing analysis demonstrated that the expression levels of proneural and neuronal marker genes were almost unchanged between the control and *miR-124a-1/2* DKO brains; however, genes related to neuronal synaptic formation and function were enriched among downregulated genes in the *miR-124a-1/2* DKO brain. In addition, we found the transcription regulator Tardbp/TDP-43, loss of which leads to defects in neuronal maturation and function, was inactivated in the *miR-124a-1/2* DKO brain. Furthermore, *Tardbp* knockdown suppressed neurite extension in cultured neuronal cells. We also generated *miR-124a-1/2/3* TKO ES cells using CRISPR-Cas9 as an alternative to TKO mice. Phase-contrast microscopic,

immunocytochemical, and gene expression analyses showed that *miR-124a-1/2/3* TKO ES cell lines were able to differentiate into neurons.

Collectively, these results show that *miR-124a* plays a role in neuronal maturation rather than neurogenesis *in vivo* and advance our understanding of the functional roles of microRNAs in vertebrate CNS development.

Table of Contents

Introduction

Of the human genome, only less than 2% is transcribed into protein-coding RNA (mRNA) (Fig. 1A) (1). The rest is also mostly transcribed, however into non-coding RNAs including microRNAs (miRNAs), small RNAs, and long RNAs (Fig. 1A) (1). MicroRNAs (miRNAs) are small non-coding RNA molecules regulating the gene expression of a variety of biological processes in plants and animals. *Lin-4* was the first discovered miRNA in *Caenorhabditis elegans* (*C. elegans*) in 1993 (Fig. 1B) (2, 3). Seven years later, *let-7* was discovered as the second miRNA and reported to be evolutionarily

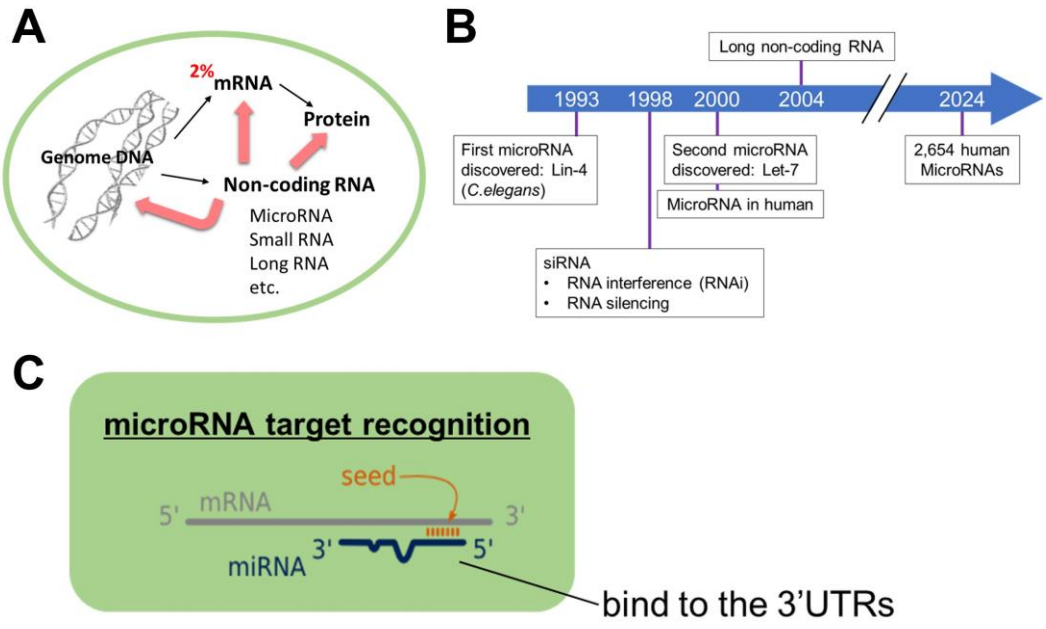

Figure 1. miRNAs

(A) Schematic diagram of central dogma and non-coding RNA. Of the human genome, only less than 2% is transcribed into protein-coding RNA (mRNA) and the rest is also mostly transcribed, however into non-coding RNAs including miRNAs, small RNAs, and long RNAs. **(B)** Historical perspective on the discovery of non-coding RNA, mainly miRNAs. **(C)** miRNAs bind to the 3' UTRs of their target mRNAs and interfere with translation or degrade mRNAs. The seed sequence is important for binding to the target.

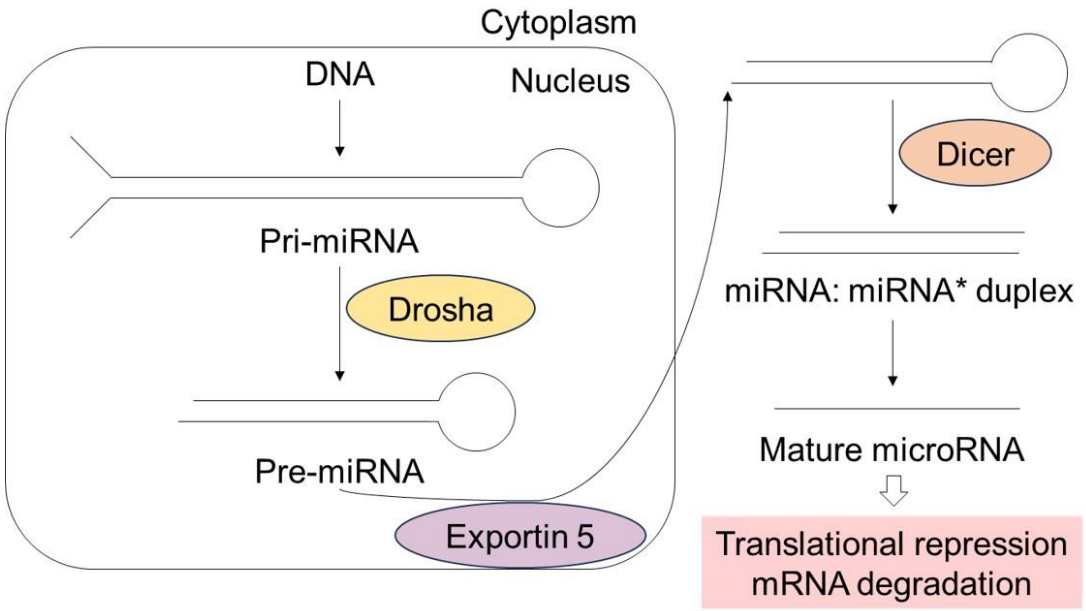

Figure 2. Generation of miRNAs
miRNAs are transcribed as primary transcripts (pri-miRNAs) from the genome. The pri-miRNA transcripts are firstly processed into ~70-nucleotide pre-miRNAs by Drosha, an Rnase-III enzyme, inside the nucleus. Pre-miRNAs are transported to the cytoplasm by Exportin 5 and further processed into miRNA:miRNA* duplexes by Dicer, another Rnase-III enzyme. Only one strand of the miRNA:miRNA* duplexes functions as ~21–25-nucleotide mature miRNA.

well conserved throughout metazoans including human (Fig. 1B) (4). This extensive conservation suggested a more general role of miRNAs in various organisms. To date, 2,654 human mature miRNAs have been identified (Fig. 1B) (5). In many cases, miRNAs bind to their target 3' UTRs through imperfect complementarity at multiple sites except for seed sequence and interfere translation and/or degrade mRNAs (Fig. 1C). Two processing events contribute to miRNAs formation in animals (6). First, pri-miRNA is transcribed from the genome and processed into ~70-nucleotide precursors (pre-miRNA) (Fig. 2). Secondly, pre-miRNA is cleaved to generate ~21–25 nucleotide mature miRNAs

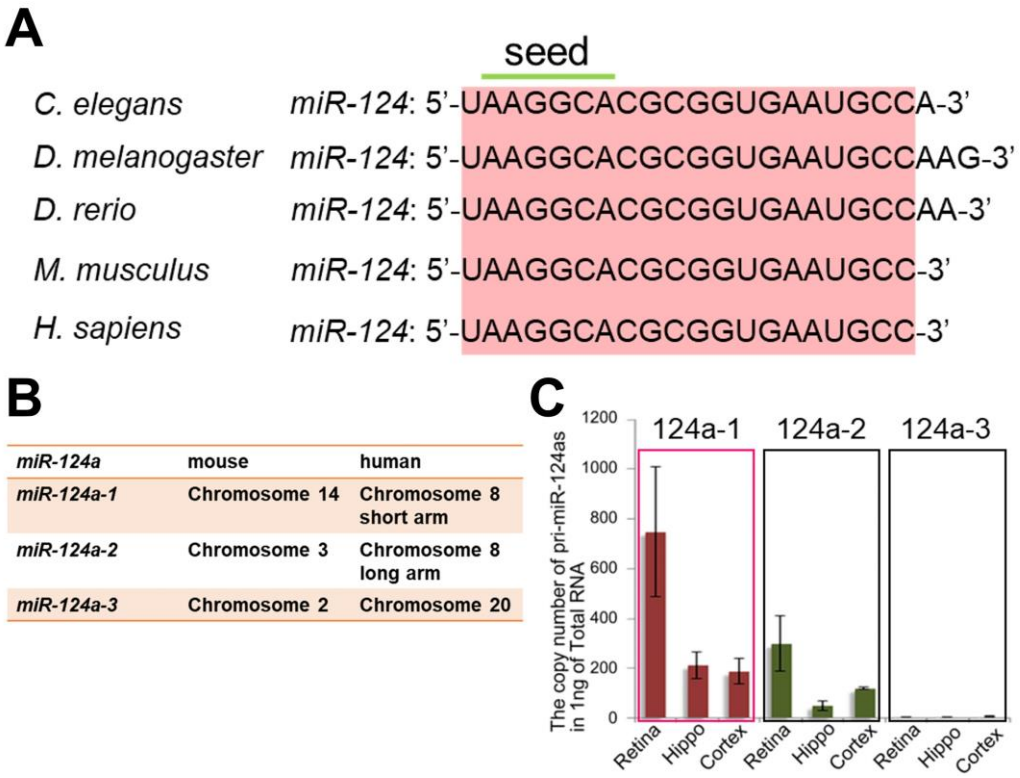

miR-124a	mouse	human
miR-124a-1	Chromosome 14	Chromosome 8 short arm
miR-124a-2	Chromosome 3	Chromosome 8 long arm
miR-124a-3	Chromosome 2	Chromosome 20

Figure 3. Neuronal miRNA, *miR-124a*

(A) The nucleotide sequence of *miR-124a* is evolutionarily highly conserved from *C. elegans* to human. **(B)** Both in human and mouse genomes, *miR-124as* are encoded by three differential chromosome loci: *miR-124a-1*, *-2*, and *-3*. **(C)** Quantitative RT-PCR analysis of *pri-miR-124as* in the retina, hippocampus, and cortex of P6 WT mice (modified from Supplementaly Fig. 1b (8)). Among the three *pri-miR-124as*, *pri-miR-124a-1* is predominantly expressed while *pri-miR-124a-3* is barely expressed in the CNS of mice.

(Fig. 2). A large number of diverse miRNAs are expressed in the vertebrate central nervous system (CNS). *MicroRNA-124a* (*miR-124a*) is one of the most abundantly expressed miRNAs in mouse and human brains (7). The nucleotide sequence of *miR-124a* and its nervous system-specific expression pattern are evolutionarily highly conserved from *C. elegans* and *Drosophila melanogaster* to all studied vertebrates, including human (Fig. 3A). Both in human and mouse genomes, *miR-124as* are encoded by three loci: *miR-124a-1*, *-2*, and *-3* (Fig. 3B). Among the three primary *miR-124as* (*pri-miR-124as*), *pri-*

miR-124a-1 is predominantly expressed while *pri-miR-124a-3* is barely expressed in the mouse brain (Fig.3C) (8). In mice, we found that *Retinal non-coding RNA 3* (*RNCR3*) functions as a *pri-miR-124a-1* precursor. We previously identified *RNCR3* in the mouse retina and generated *RNCR3*-deficient mice (*RNCR3*$^{-/-}$) by deleting the entire 4.5 kb region harboring *RNCR3* (8). Since we confirmed that a loss of *miR-124a* is responsible for the *RNCR3*$^{-/-}$ abnormalities by *in vivo* rescue experiments in our previous study, we will refer to *RNCR3*$^{-/-}$ mice as *miR-124a-1*$^{-/-}$ mice in the current study. In the *miR-124a-1*$^{-/-}$ brain, the level of mature *miR-124a* was reduced by 60–80 % compared with that in the wild-type (WT) control brain. *miR-124a-1*$^{-/-}$ mice showed abnormalities in the CNS such as over-extension of the dentate gyrus granule neuron axons and apoptosis of cone photoreceptor cells in the retina at the stages after neurogenesis; however, these phenotypes were not apparent at the developmental stages (8), suggesting that *miR-124a-1* is essential for neuronal maturation rather than neurogenesis (Fig. 4A). *miR-124a-1* is localized in the chromosome 8p23.1 region in the human genome. It was reported that heterozygous deletions in the human 8p23.1 region are related to psychiatric disorders such as schizophrenia, autism, and social impairment (9–12). We subjected *miR-124a-1*$^{+/-}$ mice to a comprehensive behavioral battery and found that *miR-124a-1*$^{+/-}$ mice exhibited social defects, methamphetamine-induced hyperactivity, and impaired prepulse inhibition (Fig. 4A). Our previous study showed that *miR-124a-1* regulates prefrontal cortex function by dopaminergic modulation (13).

In *C. elegans miR-124* mutants, neurons are normally generated and no overt phenotype is observed (14, 15). *Drosophila miR-124* mutants exhibit abnormalities in neuroblast proliferation and neuronal maturation (16, 17). In vertebrates, consistent with its expression pattern in the developing CNS, *miR-124a* has been reported to be essential

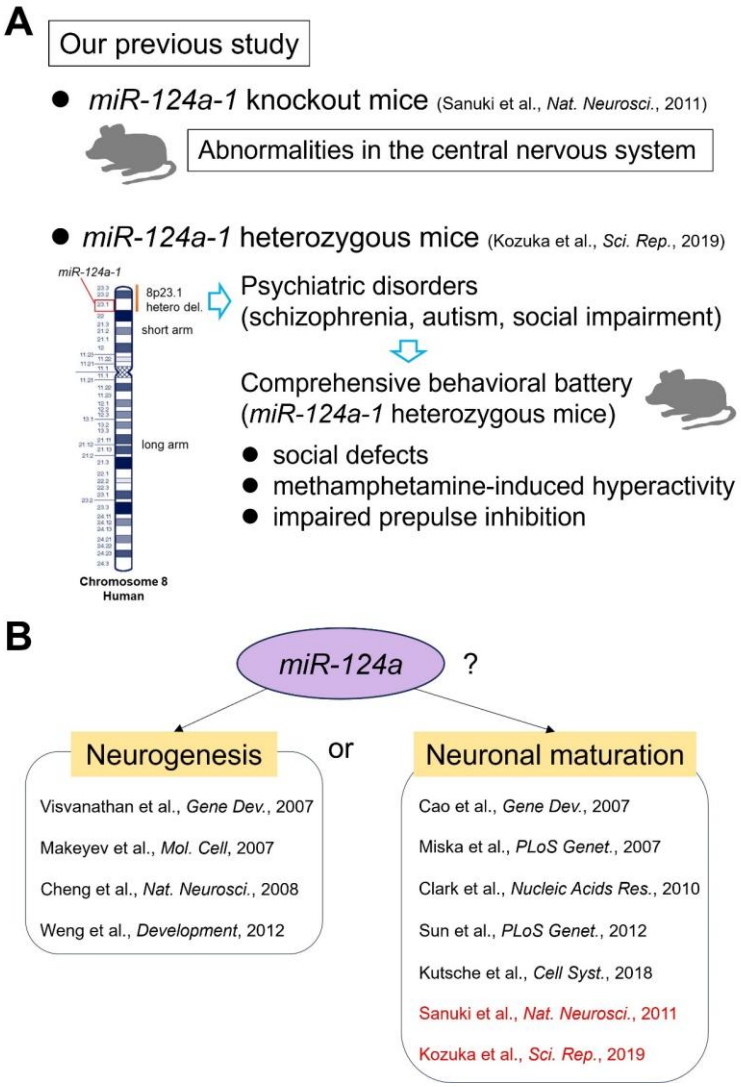

Figure 4. Our and others previous studies on *miR-124a*

(A) Schematic diagrams of previous studies on *miR-124a* function in our laboratory. We generated and analyzed *miR-124a-1*$^{-/-}$ mouse line, suggesting that *miR-124a-1* is essential for neuronal maturation rather than neurogenesis. **(B)** Is *miR-124a* required for neurogenesis or neuronal maturation? Conflicting results on *miR-124a* function had been reported. In the current study, we investigated the effect of *miR-124a* loss on neuronal differentiation in mice and in embryonic stem (ES) cells by generating and analyzing multiple knockout models.

for neurogenesis (18, 19), maturation (8, 20–22), and progenitor proliferation (18). However, it should be noted that conflicting results on *miR-124a* function have been reported (Fig. 4B). It was reported that neither inhibition nor overexpression of *miR-124a*

affects neuronal differentiation or progenitor proliferation in the chick neural tube (20). Overexpression of transcription factors, Neurog1 and Neurog2, and a small molecule-based culture condition can induce neuronal differentiation from human induced pluripotent stem cells deficient for *miR-124a* (23). On the other hand, other studies reported that *miR-124a* promotes both embryonic and adult neurogenesis (18, 24). In the chick spinal cord, *miR-124a* was implicated in the stimulation of neuronal differentiation by suppressing the anti-neuronal REST/SCP1 pathway. In addition, *miR-124a* induces neurogenesis in P19 mouse embryonic cells (18). In the adult mouse subventricular zone, *miR-124a* was shown to induce adult neurogenesis through the regulation of Sox9 (24). Using *miR-124a-1*$^{-/-}$ mouse line, we have demonstrated that *miR-124a* plays a crucial role in neuronal maturation rather than neurogenesis; however, *miR-124a-2* and *miR-124a-3* may have the ability to induce neurogenesis. Based on these various reports, in the current study, we investigated the role of *miR-124a* in neuronal development by generating and analyzing *miR-124a-1/2* double knockout (DKO) mice and *miR-124a-1/2/3* triple knockout (TKO) cells.

Results

Generation of multiple *miR-124a* knockout mice

To investigate the *in vivo* function of *miR-124a* paralogs, we first generated *miR-124a-2*$^{-/-}$ mice, which harbor a deletion that includes the entire *pre-miR-124a-2* sequence on mouse chromosome 3 (Fig. 5A). We also generated *miR-124a-3*$^{-/-}$ mice by deleting a fragment containing the entire *pre-miR-124a-3* sequence on chromosome 2 (Fig. 5B). We confirmed deletions by Southern blot analysis using genomic DNA from these mice (Fig. 5C-F). Both *miR-124a-2*$^{-/-}$ and *-3*$^{-/-}$ mice were viable and fertile. Coronal sections of

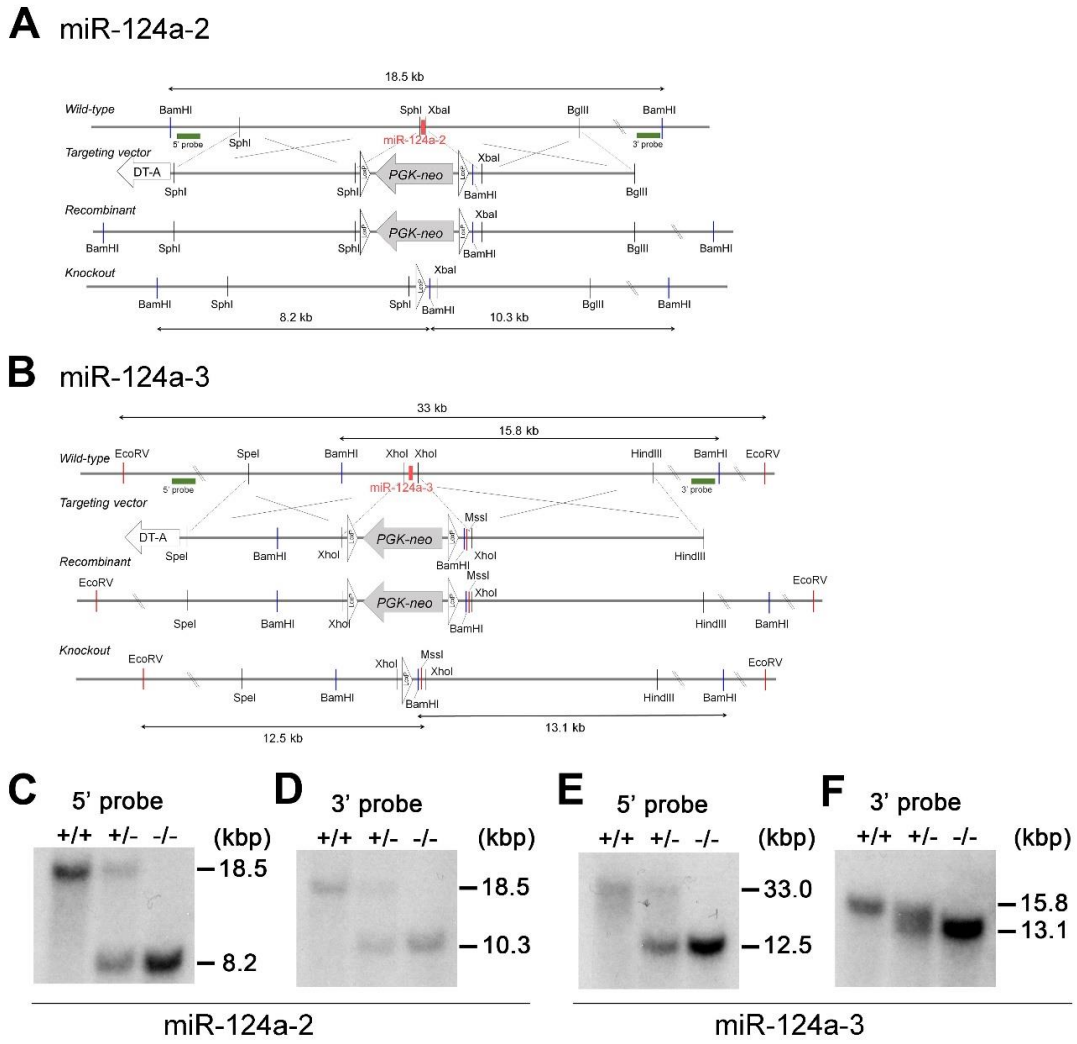

Figure 5. Generation of *miR-124a-2*$^{-/-}$ *and -3*$^{-/-}$ mice.
(A, B) Diagrams of the targeting vectors and the *miR-124a-2*$^{-/-}$ *and -3*$^{-/-}$ alleles. The *miR-124a-2*$^{-/-}$ (A) and *-3*$^{-/-}$ (B) alleles are shown. Genomic regions encoding *miR-124a-2* and *-3* precursors are replaced by floxed *PGK-neo* cassettes. **(C-F)** Southern blot analysis of genomic structure of *miR-124a-2* and *-3* loci. BamHI- (C, D, F) or EcoRV/MssI-digested (E) genomic DNA was hybridized with 5′(C, E) and 3′ probes (D, F) for *miR-124a-2* (C, D) and *-3* loci (E, F). The 5′ probe of *miR-124a-2* detected 18.5-kb WT and 8.2-kb mutant bands (C). The 3′ probe of *miR-124a-2* detected 18.5-kb WT and 10.3-kb mutant bands (D). The 5′ probe of *miR-124a-3* detected 33.0-kb WT and 12.5-kb mutant bands (E). The 3′ probe of *miR-124a-3* detected 15.8-kb WT and 13.1-kb mutant bands (F).

miR-124a-2$^{-/-}$ and *miR-124a-3*$^{-/-}$ brains showed no obvious morphological changes compared with the WT control brain (Fig. 6). Next, we compared *miR-124a-2*$^{-/-}$ and miR-124a-3$^{-/-}$ brains with *miR-124a-1*$^{-/-}$ brain. In contrast to the previously described decreased brain weight of *miR-124a-1*$^{-/-}$ mice (8), *miR-124a-2*$^{-/-}$ and *-3*$^{-/-}$ mice exhibited no brain weight change at 2 months of age (2M) (Fig. 7A). While *miR-124a-2*$^{-/-}$ and *-3*$^{-/-}$ brains showed no apparent changes compared with the WT control brain, thickness of the cerebral cortex decreased in the *miR-124a-1*$^{-/-}$ brain (Figs. 7B). Aberrant outgrowth of mossy fibers stained with Calbindin (CALB1) into the hippocampal CA3 region was observed in *miR-124a-1*$^{-/-}$ mice as previously described (Fig. 7C) (8). In contrast, the morphology of mossy fibers in the *miR-124a-2*$^{-/-}$ and *-3*$^{-/-}$ hippocampi were not substantially different from that in the WT control hippocampus (Fig. 7C). These results suggest that *miR-124a-2* and *-3* have a minor role in brain development compared with *miR-124a-1*.

Next, to investigate the effect of the complete loss of *miR-124a in vivo* by analyzing *miR-124a-1/2/3* TKO mice, we generated *miR-124a-1/2* double heterozygous (DHet) and then *miR-124a-1/2/3* triple heterozygous (THet) mice by mating. We examined whether

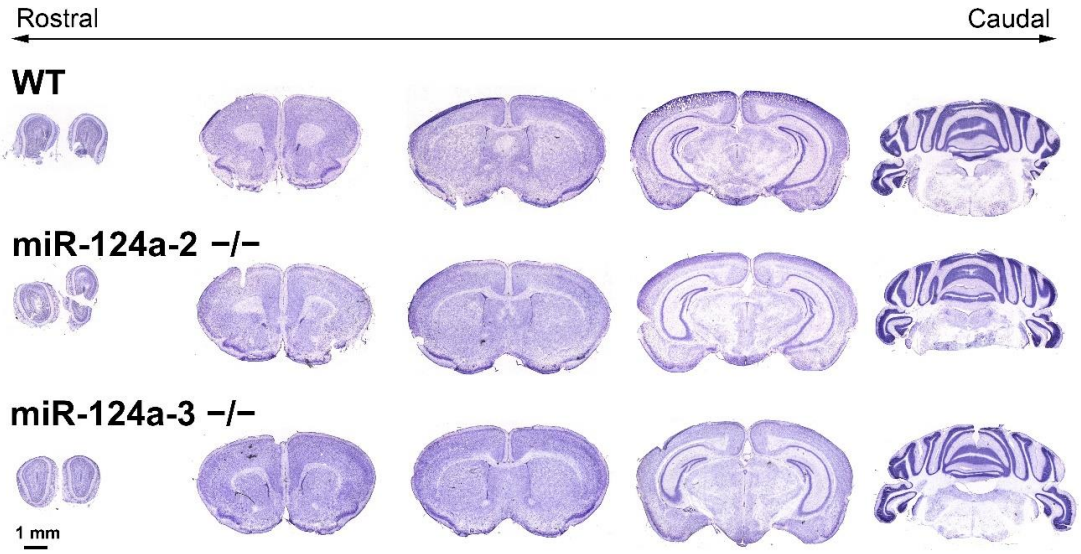

Figure 6. Coronal sections from the WT control, *miR-124a-2*$^{-/-}$, and -*3*$^{-/-}$ brains. Nissl staining of serial brain sections arranged from rostral to caudal of the WT control, *miR-124a-2*$^{-/-}$, and -*3*$^{-/-}$ mice at 2M.

miR-124a paralog multiple heterozygosity affects postnatal growth. We measured body weights of *miR-124a-1/2* DHet and *miR-124a-1/2/3* THet mice, and found that *miR-124a-1/2* DHet and *miR-124a-1/2/3* THet mice both exhibit growth retardation (Fig. 7D). At 8 weeks (wks) *miR-124a-1/2* DHet and *miR-124a-1/2/3* THet mice were 83 % and 68 % smaller than WT control mice, respectively. Brain weights of *miR-124a-1/2* DHet and *miR-124a-1/2/3* THet mice at 8 wks were significantly smaller than those of WT control mice (81 % and 72 %, respectively) (Fig. 7E). Although we first attempted to generate *miR-124a-1/2/3* TKO mice, we could not obtain progeny by mating *miR-124a-1/2/3* THet mice. Since *pri-miR-124a-2* is the second major source of *miR-124a* after *pri-miR-124a-1*, and *pri-miR-124a-3* is barely expressed in the brain (8), we next tried to generate *miR-124a-1/2* DKO mice by mating *miR-124a-1/2* DHet mice. Both male and female *miR-124a-1/2* DHet mice were fertile. We found that *miR-124a-1/2* DKO mice show perinatal lethality, suggesting severe abnormalities in the CNS of *miR-124a-1/2* DKO mice.

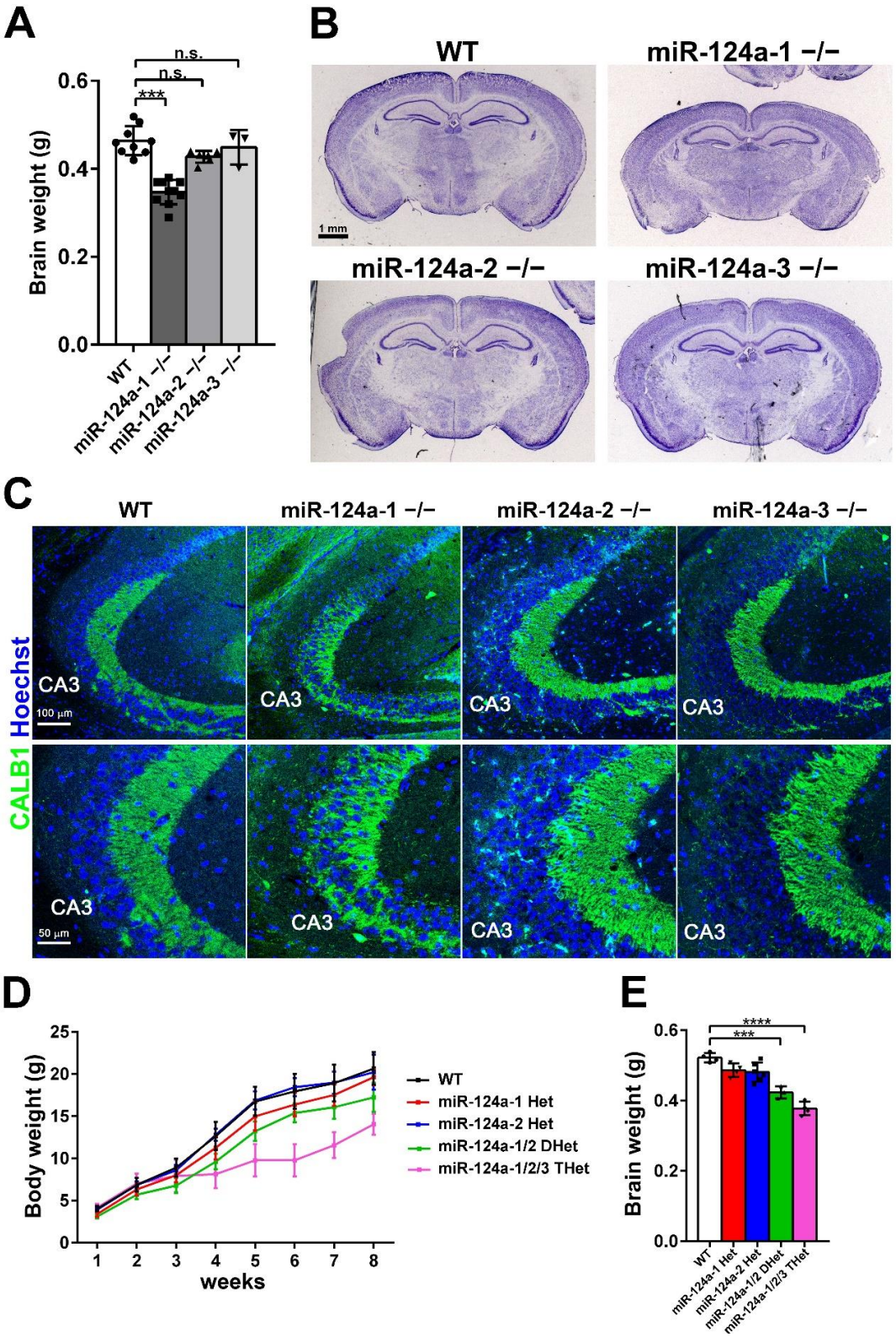
A
n.s.
n.s.
***
Brain weight (g)
0.6
0.4
0.2
0.0
WT
miR-124a-1 −/−
miR-124a-2 −/−
miR-124a-3 −/−
B
WT
miR-124a-1 −/−
1 mm
miR-124a-2 −/−
miR-124a-3 −/−
C
WT
miR-124a-1 −/−
miR-124a-2 −/−
miR-124a-3 −/−
CALB1 Hoechst
CA3
100 µm
50 µm
D
Body weight (g)
25
20
15
10
5
0
1
2
3
4
5
6
7
8
weeks
WT
miR-124a-1 Het
miR-124a-2 Het
miR-124a-1/2 DHet
miR-124a-1/2/3 THet
E
****
***
Brain weight (g)
0.6
0.4
0.2
0.0
WT
miR-124a-1 Het
miR-124a-2 Het
miR-124a-1/2 DHet
miR-124a-1/2/3 THet

Figure 7. Anatomical analysis of the *miR-124a* mutant mouse brain.
(A) Brain weight of WT control, *miR-124a-1*$^{-/-}$, *-2*$^{-/-}$, or *-3*$^{-/-}$ mice at 2M. Data are presented as the mean ± SD. $^{***}p < 0.001$; n.s., not significant (one-way ANOVA followed by Tukey-Kramer test), n = 3–10 per genotype. **(B)** Nissl-stained coronal sections of the brain from WT control, *miR-124a-1*$^{-/-}$, *-2*$^{-/-}$, or *-3*$^{-/-}$ mice at 2M. Thinning of the cerebral cortex was observed in the *miR-124a-1*$^{-/-}$ brain. **(C)** Immunofluorescent staining of hippocampi from WT control, *miR-124a-1*$^{-/-}$, *-2*$^{-/-}$, and *-3*$^{-/-}$ mice at 2M. Mossy fibers were immunostained with an anti-CALB1 antibody (green). **(D)** Body weight of WT control, *miR-124a-1*$^{+/-}$, *-2*$^{+/-}$, *-1/2* DHet, and *-1/2/3* THet mice was measured weekly for 8 wk after birth. Data are presented as the mean ± SD. n = 4–11 per genotype. **(E)** Brain weight of WT control, *miR-124a-1*$^{+/-}$, *-2*$^{+/-}$, *-1/2* DHet, and *-1/2/3* THet mice was measured at 2M. Data are presented as the mean ± SD. $^{***}p < 0.001$, $^{****}p < 0.0001$ (one-way ANOVA followed by Tukey-Kramer test), n = 3–6 per genotype.

Embryonic brain development is perturbed in *miR-124a-1/2* DKO mice

To assess the consequence of *miR-124a-1/2* deficiency on CNS development, we performed RNA-sequencing (RNA-seq) analysis using total RNAs purified from three control (*miR-124a-1*$^{+/-}$) and three *miR-124a-1/2* DKO mouse brains at embryonic day 17.5 (E17.5) (Fig. 8). There were no obvious differences between WT control and *miR-124a-1/2* DKO embryos at E17.5 (Fig. 8A). We confirmed that *miR-124a* target genes are enriched in the up-regulated genes in the *miR-124a-1/2* DKO brain (adjusted p = 1.8 × 10-7) (Fig. 8B). We first examined the gene expression of *NeuroD1* (a proneural marker), *Map2* (a mature neuronal marker), *Gad2* (a GABAergic neuronal marker), *VGluT1* (a glutamatergic neuronal marker), and *Tuj1* (an early neuronal marker) in the control and *miR-124a-1/2* DKO brains. Although the expression level of *Tuj1* was significantly but slightly decreased in the *miR-124a-1/2* DKO brain, that of other examined markers was not significantly changed, suggesting that neurogenesis occurs in the *miR-124a-1/2* DKO brain (Fig. 8C).

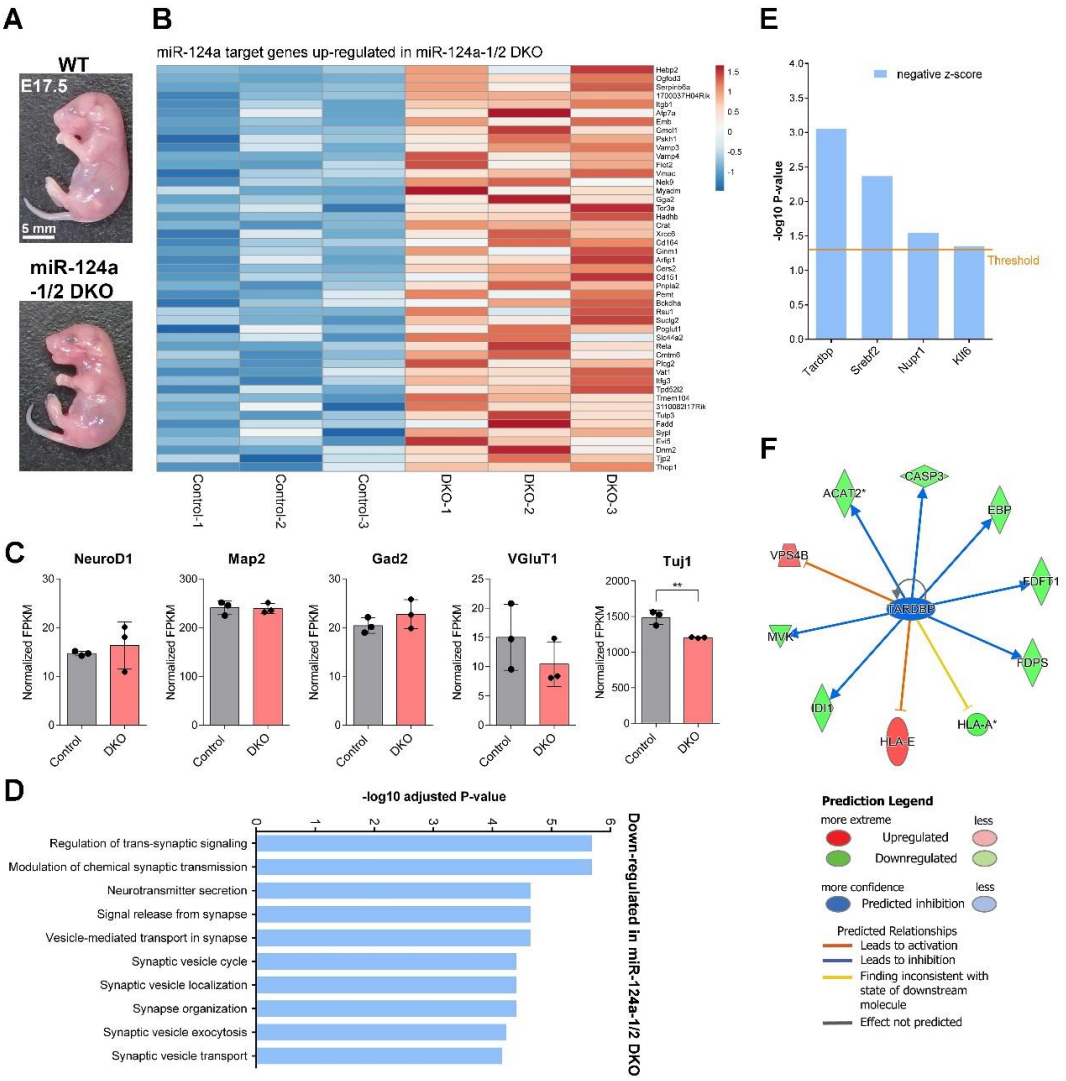

Classification of the down-regulated genes in the *miR-124a-1/2* DKO brain into functional categories according to the Gene Ontology (GO) term enrichment for the Biological Process showed that these genes are associated with processes related to neuronal synaptic formation and function (Fig. 8D). These results imply that *miR-124a* plays a role in neuronal maturation and function rather than neurogenesis.

We next searched for the upstream transcription regulators that affect gene expression changes observed in the *miR-124a-1/2* DKO brain. Ingenuity Pathway Analysis (IPA) revealed that the transcription regulators Tardbp/TDP-43, Srebf2, Nupr1, and Klf6 are inactivated by *miR-124a-1/2* deficiency (Z scores < −2) (Fig. 8E, F). We examined the

Figure 8. RNA-seq analysis of the *miR-124a-1/2* DKO mouse brain.

(A) Images of WT control and *miR-124a-1/2* DKO mouse embryos at E17.5. **(B)** Heatmaps of the *miR-124a* target genes up-regulated in *miR-124a-1/2* DKO mouse brains at E17.5 compared with those in the control (*miR-124a-1*$^{+/-}$) mouse brains (fold change > 1.2; $p < 0.05$, unpaired t-test). Gene expression values are visualized using a color scale from blue to red. Fragments per kilobase of exon per million mapped fragment values from the RNA-seq dataset were used for the heatmap visualization. **(C)** Gene expression levels of *NeuroD1*, *Map2*, *Gad2*, *VGluT1*, and *Tuj1* (neuronal markers) in the control and *miR-124a-1/2* DKO brains at E17.5. Data are presented as the mean ± SD. $^{**}p < 0.01$ (unpaired t-test), n = 3 per genotype. **(D)** The top 10 most significantly enriched biological processes determined by gene ontology enrichment analysis for down-regulated genes in the *miR-124a-1/2* DKO brain compared with those in the control brain using iDEP. X-axis indicates $-\log_{10}$ adjusted P-value and Y-axis indicates biological processes. **(E)** IPA to predict the upstream transcription regulators affecting gene expression changes ($p < 0.05$, unpaired t-test) in the *miR-124a-1/2* DKO brain. The transcription regulators with activation Z scores < −2 are shown.**(F)** IPA networks showing the transcription factor Tardbp as an upstream regulator. Tardbp is predicted to be inactivated in the *miR-124a-1/2* DKO brain.

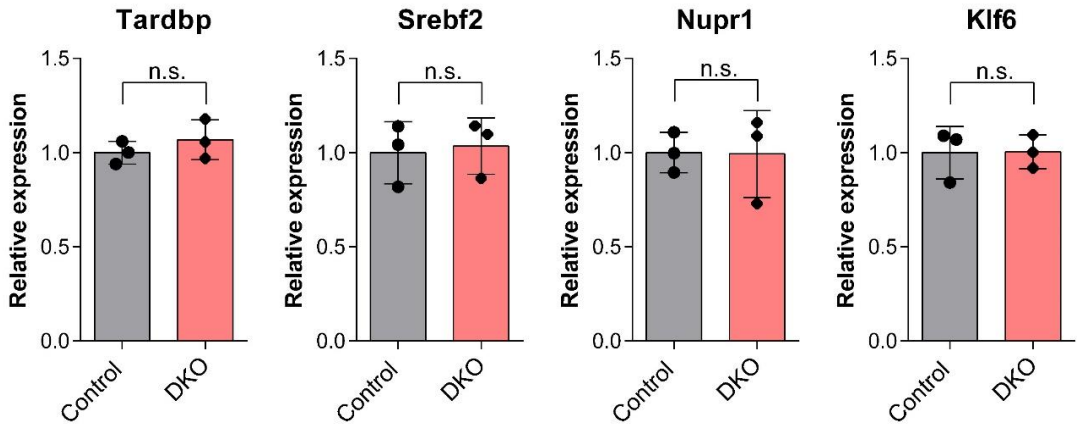

Figure 9. Expression levels of genes encoding transcription regulators in the *miR-124a-1/2* DKO mouse brain.

Quantitative RT-PCR analysis of the *Tardbp*, *Srebf2*, *Nupr1*, and *Klf6* mRNAs in the control and *miR-124a-1/2* DKO brains at E17.5. Data are presented as the mean ± SD. n.s., not significant (unpaired t-test), n = 3 per genotype.

gene expression of *Tardbp*, *Srebf2*, *Nupr1*, and *Klf6* by qRT-PCR and found that there are no significant differences between the control and *miR-124a-1/2* DKO brains (Fig. 9),

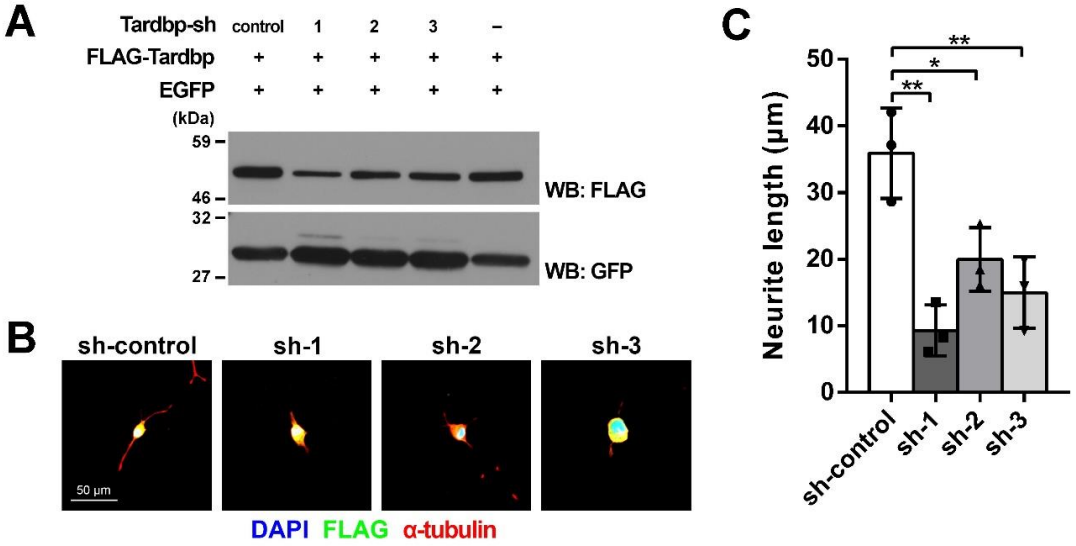

Figure 10. Roles of Tardbp on neurite extension in cultured neuronal cells.

(A) Inhibition efficacy of shRNA expression constructs for *Tardbp* knockdown. ShRNA-control, Tardbp-shRNA1, Tardbp-shRNA2, or Tardbp-shRNA3 expression plasmids were co-transfected with plasmids expressing a FLAG-tagged Tardbp and a GFP into HEK293T cells. Western blot analysis was performed using anti-FLAG and anti-GFP antibodies. GFP was used as an internal transfection control. Tardbp-shRNA1, Tardbp-shRNA2, and Tardbp-shRNA3 suppressed Tardbp expression. **(B, C)** ShRNA-control, Tardbp-shRNA1, Tardbp-shRNA2, or Tardbp-shRNA3 expression plasmids were co-transfected with a plasmid expressing FLAG-tagged EGFP into Neuro2a cells. Cells were immunostained with anti-FLAG and anti-α-tubulin antibodies. Nuclei were stained with DAPI (B). The length of the longest neurite of the transfected cells was measured (C). Data are presented as the mean ± SD. *$p < 0.05$, **$p < 0.01$ (one-way ANOVA followed by Tukey-Kramer test), n = 3 experiments. A total of 63, 25, 59, and 55 cells were measured in shRNA-control, Tardbp-shRNA1, Tardbp-shRNA2, and Tardbp-shRNA3, respectively.

suggesting that the transcription regulators Tardbp, Srebf2, Nupr1, and Klf6 are down-regulated at the protein level. Among the genes encoding these transcription regulators, loss of function of *Tardbp* is known to lead to neuronal axon defects, impaired synaptic transmission, neuronal death, and motor deficit *in vivo* (25, 26). Furthermore, *Tardbp* knockout mice exhibit embryonic lethality (27–29). To examine the roles of Tardbp in neuronal maturation, we performed knockdown experiments using Neuro2a cells. We

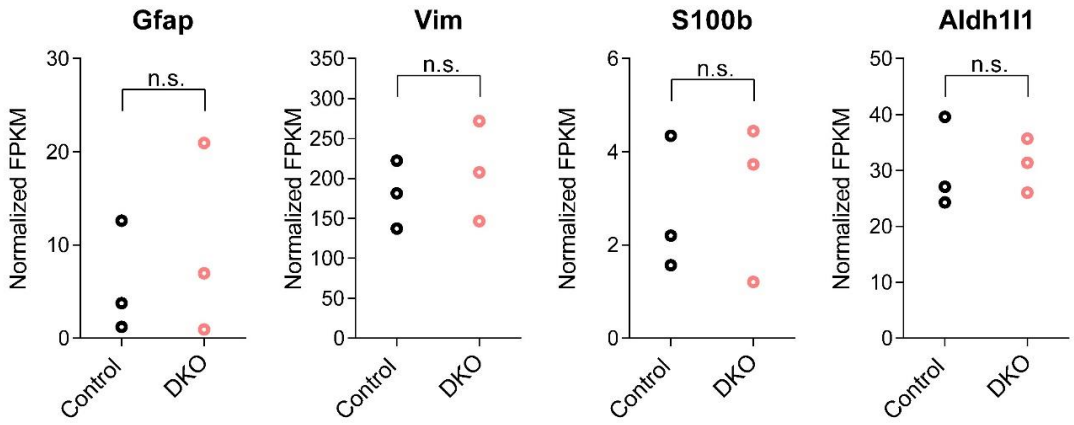

Figure 11. Gene expression analysis of glial markers in the *miR-124a-1/2* DKO mouse brain.

Gene expression levels of *Gfap*, *Vim*, *S100b*, and *Aldh1l1* (radial glia and/or astrocyte markers) in the control and *miR-124a-1/2* DKO brains at E17.5. n.s., not significant (unpaired t-test), n = 3 per genotype.

first constructed short hairpin RNAs (shRNAs) to knockdown *Tardbp* and confirmed that the Tardbp expression levels decrease in the cells expressing Tardbp-shRNA1, -shRNA2, and -shRNA3 (Fig. 10A). We transfected these constructs into Neuro2a cells and observed the neurites by immunostaining using anti-α-tubulin and anti-FLAG antibodies. We found that Tardbp-shRNAs significantly suppress neurite extension (Fig. 10B, C). Inactivation of *Tardbp* in the brain may be at least partly a cause of perinatal lethality of *miR-124a-1/2* DKO mice. We also examined the gene expression of *Gfap*, *Vim*, *S100b*, and *Aldh1l1* (radial glia and/or astrocyte markers). We found that there are no significant differences between the control and miR-124a-1/2 DKO brains (Fig. 11).

miR-124a-1/2/3 TKO ES cells differentiate into neurons

To investigate the effect of complete loss of *miR-124a* in neuronal development, we generated *miR-124a-1/2/3* TKO embryonic stem (ES) cells and tried to induce their differentiation into neurons. To create multiplex deletions of *miR-124a-1/2/3* loci in

Figure 12. The genomic DNA sequences of mutant alleles in *miR-124a-1/2/3* TKO ES clones #21, #71, and #93.

The mature *miR-124a* sequence is indicated in red. Deletion and insertion are shown in blue and green, respectively. Biallelic mutations in all three *miR-124a* genes were identified in clones #21, #71, and #93.

mouse ES cells, we used CRISPR/Cas9-mediated genome editing. Three clones (#21, #71, and #93) were identified as having deletions or insertions in both alleles of these three loci (Fig. 12). We tested whether these *miR-124a* TKO ES cells would differentiate into neurons by a previously established, chemically defined medium (CDM) culture system (30, 31). To confirm that *miR-124a-1/2/3* TKO cells do not express *miR-124a*, we performed northern blot analysis, and found that the expression of *miR-124a* is abolished in the *miR-124a-1/2/3* TKO cells (Fig. 13A, B). We also performed northern blot analysis using a *miR-124a* probe, and found that *miR-124a* expression increases along with

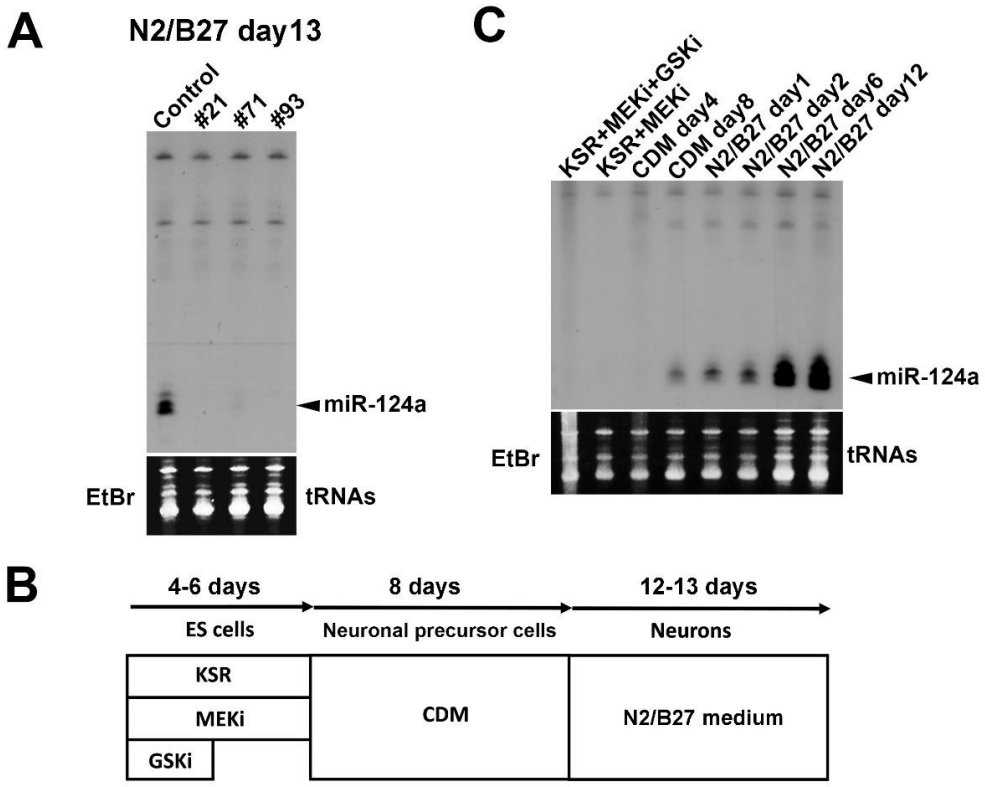

Figure 13. Neuronal differentiation of *miR-124a-1/2/3* TKO ES cells.
(A) Northern blot analysis of *miR-124a* in the control and *miR-124a-1/2/3* TKO cells. **(B)** Scheme of neuronal differentiation induction from mouse ES cells. MEKi, MEK inhibitor; GSKi, GSK3 inhibitor. **(C)** Northern blot analysis of *miR-124a* in the control cells at the indicated time points.

neuronal development in the control ES cells (Fig. 13C). The phase-contrast view shows that all three *miR-124a-1/2/3* TKO ES cell lines differentiated into aggregates of neural precursor cells in CDM and into neurons in N2/B27 medium similarly to the control ES cells (Fig. 14A). We also observed that the control and *miR-124a-1/2/3* TKO cells at N2/B27 day 1 contain Tuj1-positive cells (Fig. 14B). These results suggest that *miR-124a* is not essential for neurogenesis.

To further investigate the nature of *miR-124a-1/2/3* TKO cells, we examined the expression profiles of developmental markers in ES cells and cells at day 6 or 12 of culturing in N2/B27 medium. We observed that the expression of a stem cell marker,

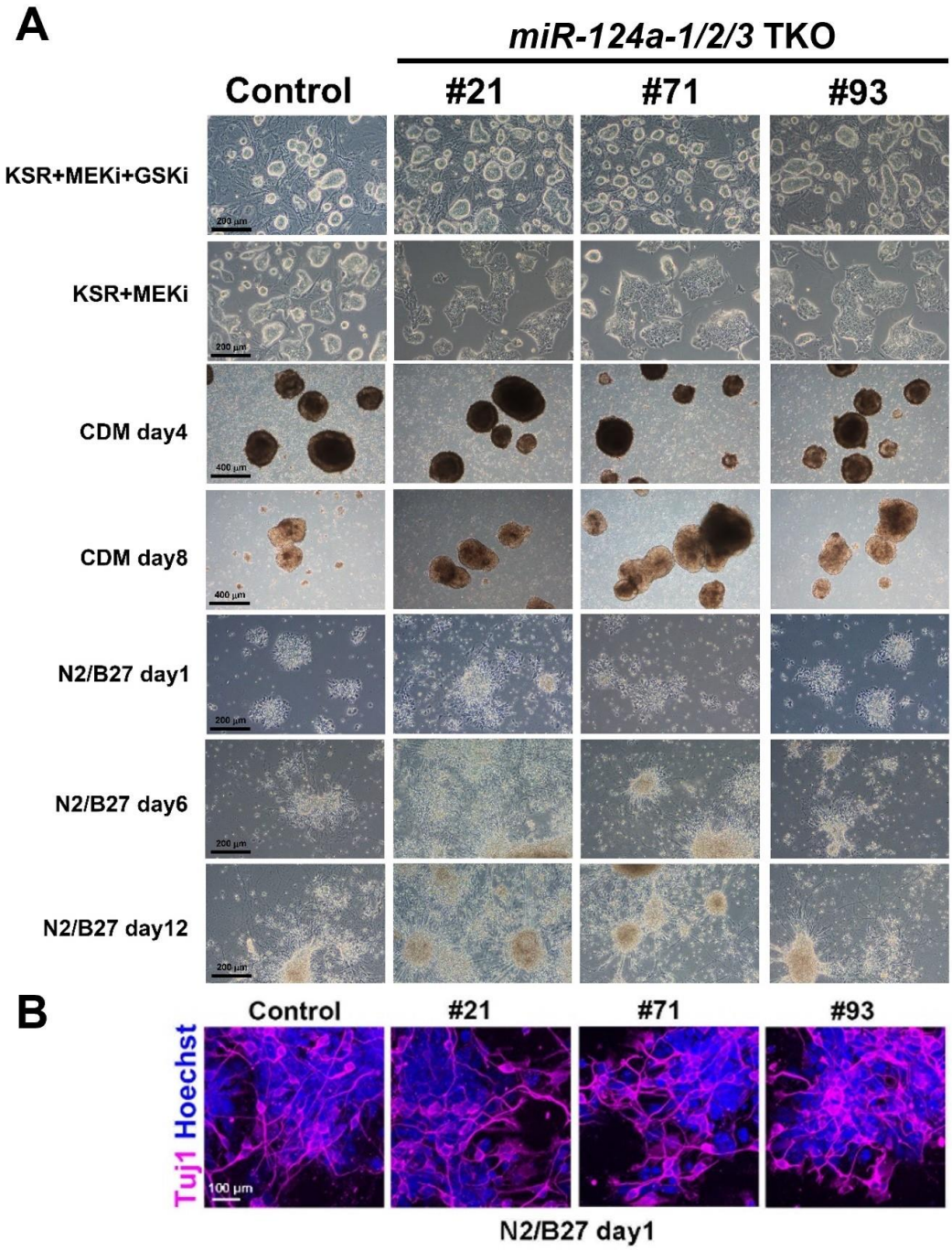

Nanog, is lost both in the control and *miR-124a-1/2/3* TKO cells at days 6 and 12 of culture in N2/B27 medium (Fig. 15A). In contrast, the expression of *NeuroD1*, *Map2*, *Gad2*, *VGluT1*, and *Tuj1* increased to similar levels both in the control and *miR-124a-1/2/3* TKO cells at days 6 and 12 of culture in N2/B27 medium (Fig. 15B–F). The

Figure 14. Phase-contrast and immunocytochemical analyses of *miR-124a-1/2/3* TKO cells during induced neuronal differentiation.

(A) Phase-contrast view of the control and *miR-124a-1/2/3* TKO cells at the indicated time points. Neuronal differentiation in the control and *miR-124a-1/2/3* TKO ES cells was induced as shown in Figure 13B. 2i, MEKi and GSKi. **(B)** Immunostaining of the control and *miR-124a-1/2/3* TKO cells at N2/B27 day 1 using an anti-Tuj1 antibody (a marker for neurons).

expression of *Gfap* was increased in the control and *miR-124a-1/2/3* TKO cells at day 12 in N2/B27 medium, although its expression levels in two of three *miR-124a-1/2/3* TKO cell lines were significantly higher than those in the control cell line (Fig. 15G). We also observed that the expression levels of one of the *miR-124a* targets, *Itgb1*, was significantly increased in *miR-124a* TKO cells compared with those in the control cells at days 6 and 12 of culture in N2/B27 medium (Fig. 15H), supporting *miR-124a* dysfunction in *miR-124a* TKO cells. Itgb1 is a major Integrin β subunit and functions in cerebral cortex development by forming heterodimers with various α subunits (32, 33). For example, the interaction between α3β1 Integrin receptor and its ligand, Reelin, regulates cortical neuronal migration (34). In addition, since the expression levels of *Gfap* in two *miR-124a-1/2/3* TKO cell lines were significantly higher than those in the control cell line at day 12 in N2/B27 medium, we examined the gene expression of *Vim*, *S100b*, and *Aldh1l1*. The expression levels of *S100b* and *Aldh1l1* increased to similar levels both in the control and *miR-124a-1/2/3* TKO cells at days 6 and/or 12 of culture in N2/B27 medium (Fig. 16). Moreover, the expression levels of *Vim* increased in the control and *miR-124a-1/2/3* TKO cells at days 6 and 12 in N2/B27 medium, although its expression levels in one or two of three *miR-124a-1/2/3* TKO cell lines were significantly higher than those in the control cell line (Fig. 16). Taken together, these results suggest that *miR-*

124a is dispensable for neurogenesis, although *miR-124a* is required for suppressing astrogenesis.

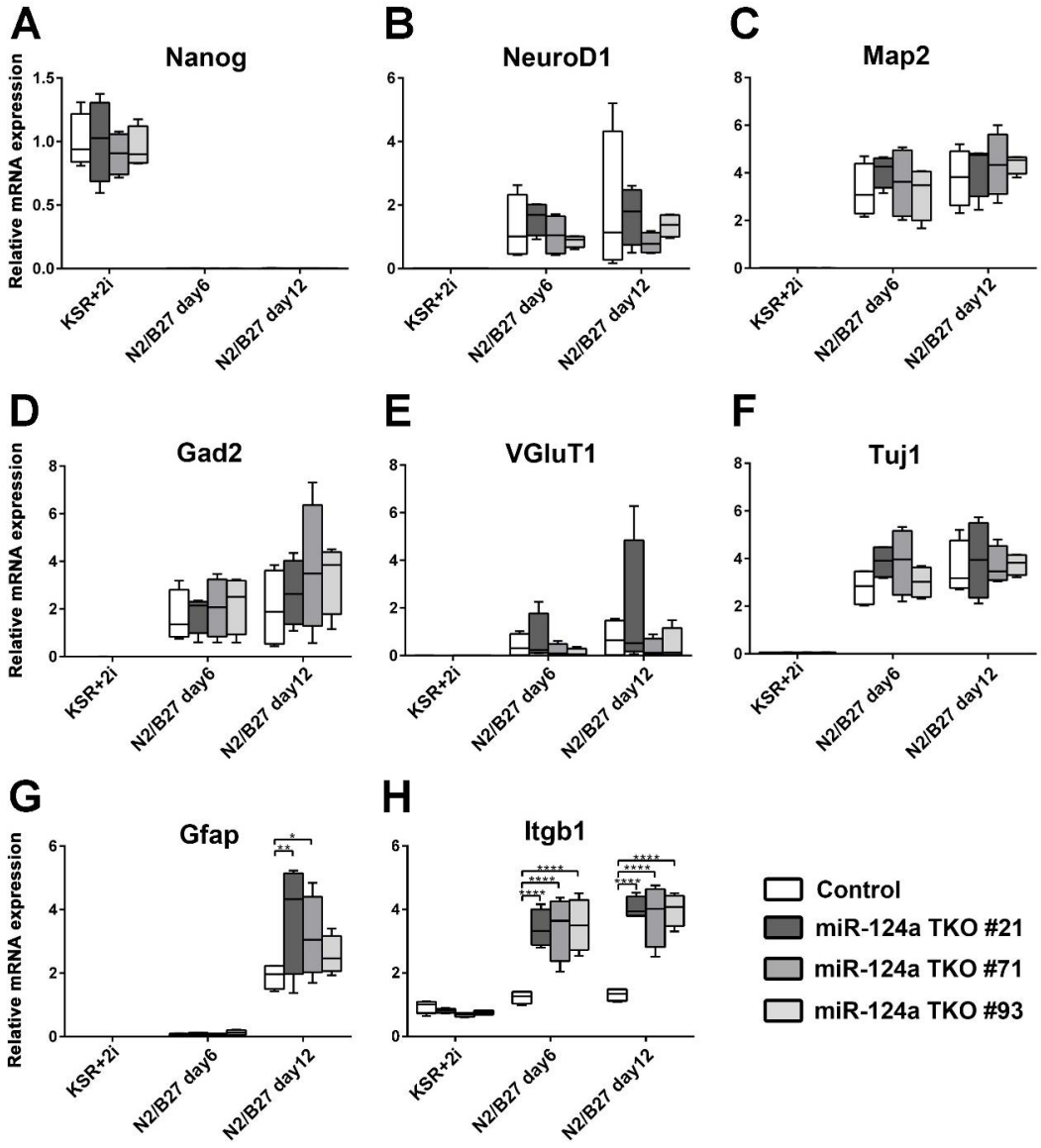

Figure 15. Gene expression analysis of neuronal differentiation-induced *miR-124a-1/2/3* TKO cells.

Expression levels of genes for a pluripotent cell marker (*Nanog*) **(A)**, neuronal markers (*NeuroD1* **(B)**, *Map2* **(C)**, *Gad2* **(D)**, *VGluT1* **(E)**, *Tuj1* **(F)**), a glial marker (*Gfap*) **(G)**, and the *miR-124a* target gene *Itgb1* **(H)** in *miR-124a-1/2/3* TKO cells at the indicated time points were analyzed. RNA was purified from cells cultured in ES medium (KSR+2i), and neuronal differentiation medium (N2/B27) for 6 or 12 days. Box–whisker plots present the median (center line), ±1.5 interquartile range (box) and minimal and maximal values (whiskers). $^{*}p < 0.05$, $^{**}p < 0.01$, $^{****}p < 0.0001$ (two-way ANOVA followed by Bonferroni test), n = 4 per cell line. 2i, MEKi and GSKi.

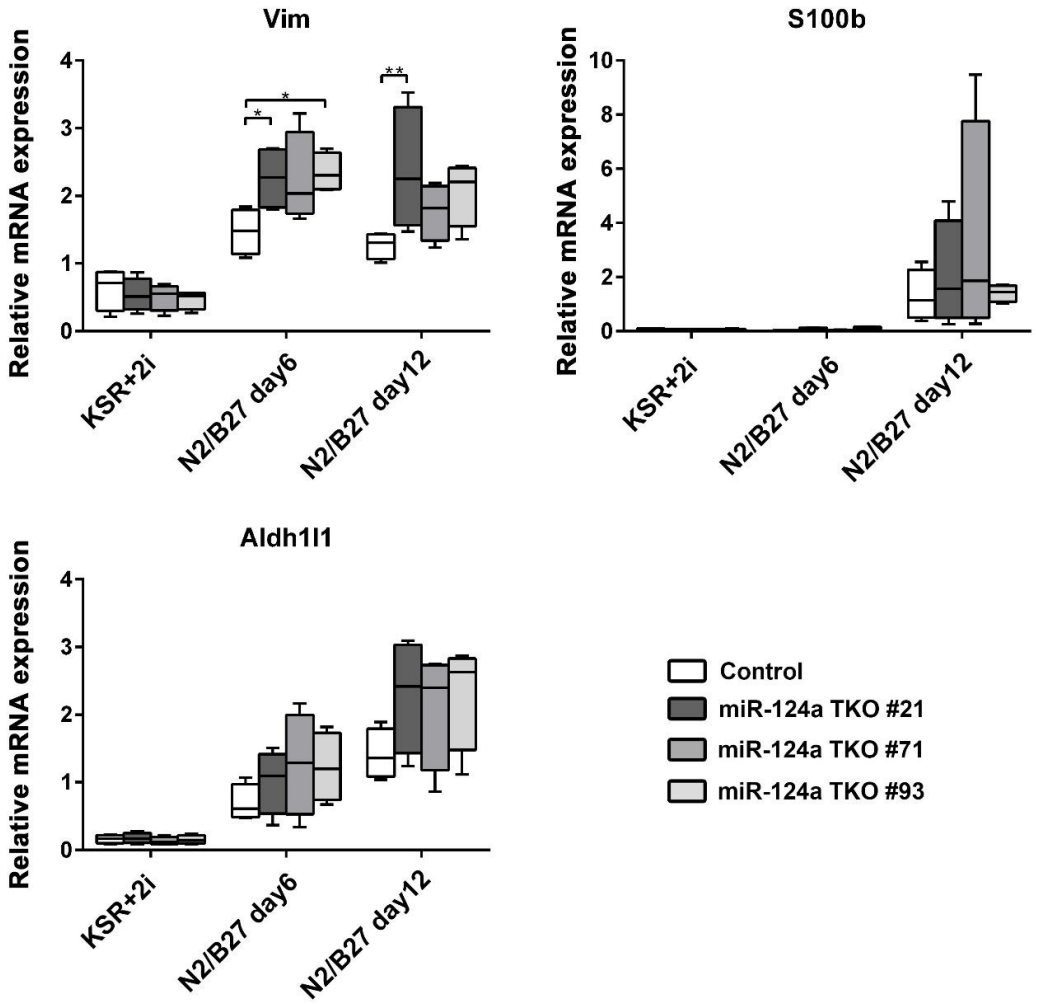

Figure 16. Gene expression analysis of glial markers in neuronal differentiation-induced *miR-124a-1/2/3* TKO cells.

Expression levels of genes for glial markers (*Vim*, *S100b*, and *Aldh1l1*) in *miR-124a-1/2/3* TKO cells at the indicated time points were analyzed. RNA was purified from cells cultured in ES medium (KSR+2i), and neuronal differentiation medium (N2/B27) for 6 or 12 days. Box–whisker plots present the median (center line), ±1.5 interquartile range (box) and minimal and maximal values (whiskers). $^{*}p < 0.05$, $^{**}p < 0.01$ (two-way ANOVA followed by Bonferroni test), n = 4 per cell line. 2i, MEKi and GSKi.

Discussion

By generating and analyzing the *miR-124a-1*$^{-/-}$ mouse line, we examined the functional roles of *miR-124a in vivo* (Fig. 4A) (8, 13); however, we cannot exclude the possibility that *miR-124a-2* and *miR-124a-3* play roles in the CNS in *miR-124a-1*$^{-/-}$ mice. Furthermore, conflicting results on *miR-124a* function have been reported; some previous studies reported that *miR-124a* is required for neurogenesis (16, 18, 19, 24), while others reported that miR-124a plays a crucial role in neuronal maturation rather than neurogenesis (Fig. 4B) (8, 14, 15, 17, 20, 23). In the current study, to further investigate the *in vivo* function of *miR-124a*, we first generated *miR-124a-2*$^{-/-}$ and *-3*$^{-/-}$ mice. Although *miR-124a-1*$^{-/-}$ mice exhibited reduced brain weight and aberrant outgrowth of mossy fibers in the hippocampus as previously described (8), *miR-124a-2*$^{-/-}$ and *-3*$^{-/-}$ mice did not show these abnormalities, suggesting that *miR-124a-2* and *-3* have minor roles in the CNS development compared with *miR-124a-1*. We also found that thickness of the cerebral cortex decreased in the *miR-124a-1*$^{-/-}$ mice, which is probably due to increased apoptosis in the *miR-124a-1*$^{-/-}$ cerebral cortex (8). Since *pri-miR-124a-1* is highly expressed in the CNS compared with *pri-miR-124a-2* and *pri-miR-124a-3* (8), abnormalities observed in the *miR-124a-1*$^{-/-}$, but not *miR-124a-2*$^{-/-}$ or *-3*$^{-/-}$ brain, may reflect their expression levels. We next attempted to investigate the consequence of the complete loss of *miR-124a in vivo*. While we could generate *miR-124a-1/2* DKO mice, in which almost all sources of *miR-124a* are depleted, we could not obtain *miR-124a-1/2/3* TKO mice by mating males and felmales of *miR-124a-1/2/3* THet mice. We thus generated *miR-124a-1/2/3* TKO ES cells using the CRISPR-Cas9 system. We observed that the expression levels of the proneural and neuronal marker genes were almost unchanged in the *miR-124a-1/2* DKO mouse brain and *miR-124a-1/2/3* TKO cells. Phase-

contrast microscopic and immunocytochemical analyses showed that neurons can differentiate from the *miR-124a-1/2/3* TKO ES cells. These results suggest that *miR-124a* is dispensable for neurogenesis, which is consistent with previous studies (8, 14, 15, 17, 20, 23). *miR-124a-1/2* DKO mice and *miR-124a-1/2/3* TKO ES cells can be a useful resource for a range of researchers interested in neuronal development and miRNA biology.

Our RNA-seq analysis demonstrated that genes associated with neuronal synaptic formation and function are enriched in down-regulated genes in the *miR-124a-1/2* DKO brain, implying that *miR-124a* is involved in neuronal maturation and function rather than neurogenesis. Notably, it was previously reported that *miR-124a* is involved in neuronal synaptic plasticity in *Aplysia* and rodents (35–37). In addition, the transcription factor Tardbp, which is required for neuronal maturation and function *in vivo* (25, 26, 38), was inactivated in the *miR-124a-1/2* DKO brain. We observed that *Tardbp* knockdown suppresses neurite extension. Notably, loss of TARDBP function is linked to the neurodegenerative diseases such as amyotrophic lateral sclerosis (ALS) and frontotemporal dementia (FTD) (39, 40). Since the expression level of *miR-124a* decreases in brain tissues from human subjects with FTD (41), the TARDBP inactivation caused by down-regulation of *miR-124a* may contribute to the pathogenesis of FTD. Together, previous studies and our current results suggest that *miR-124a* plays a role in neuronal maturation. Although we cannot rule out other explanations, up-regulated expression of a variety of *miR-124a* target genes may abrogate neuronal synaptic formation and function, inhibit Tardbp activity, and then lead to perinatal lethality in *miR-124a-1/2* DKO mice. Future analyses, such as electrophysiological and histological

evaluation, are needed to uncover how deficiency of both *miR-124a-1* and *-2* influences CNS development.

Gene expression studies of mammalian miRNAs reported that expressions of *miR-124a*, *miR-9*, *miR-125b*, and *miR-128* are enriched in the brains both at developmental and adult stages (Fig. 17) (6, 42, 43). It was previously reported that overexpression of *miR-9** and *miR-124a* causes reduced proliferation in neural progenitors, suggesting that *miR-9** and *miR-124a* have a potential to induce neuronal differentiation (44). On the other hand, our results observed in *miR-124a-1/2* DKO mice and *miR-124a-1/2/3* TKO cells suggested that *miR-124a* is dispensable for neuronal differentiation. Considering the contradiction between overexpression and deficiency of *miR-124a*, we propose several possibilities. The first hypothesis is that *miR-124a* is functionally compensated by *miR-9**. The second hypothesis is that *miR-124a* is involved in the differentiation of specific neuronal subtypes. For example, despite the low expression level, *miR-124a-3* may be able to induce neurogenesis of specific neuronal subtypes in *miR-124a-1/2* DKO mice. The third hypothesis is that the influence of *miR-124a-1/2/3* deficiency in cells is different from

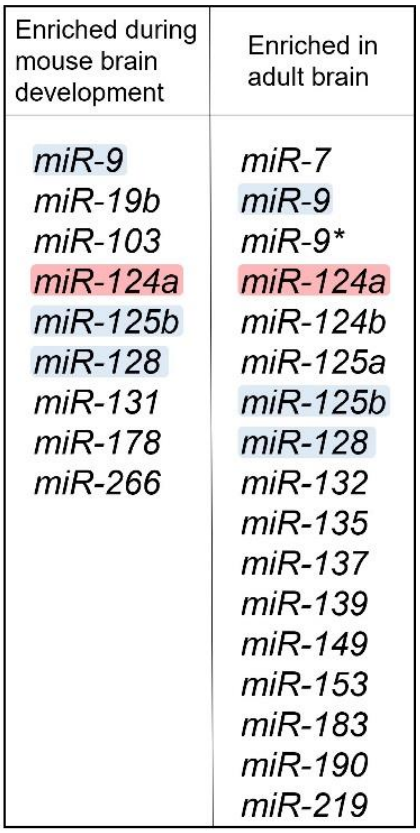

Figure 17. Expression patterns of mammalian microRNAs.
miR-124a, *miR-9*, *miR-125b*, and *miR-128* are highly expressed in the brains both at developmental and adult stages (red and blue in the figure).

that in mice. *Wnt1*-Cre-mediated *Dicer* conditional knockout mice exhibited the mostly eliminated expression of *miR-9*, *miR-124a* and *miR-218* in the midbrain and rostral hindbrain area and showed the impairment of midbrain dopaminergic neuronal differentiation (45). It may be the first hint to examine whether dopaminergic neurons differentiate abnormally in the *miR-124a-1/2* DKO brain. Furthermore, it would be important to analyze *miR-9** and *miR-124a* deficiency mice and/or *miR-124a-1/2/3* TKO mice which we may be able to generate by utilizing flox mice and to evaluate the differentiation of each neuronal subtypes in the brain in those mice. Together with the current study, these future analyses may lead to indicate unexpected notices related to the roles of *miR-124a* in neuronal differentiation.

miRNAs have been reported to be associated with various human diseases including cancers (46), cardiovascular diseases (47, 48), neurological diseases (49, 50), infectious diseases (51, 52). One of the notable challenges in the field today is to examine the effects of dysregulated miRNAs in human pathologies and explore their potential as biomarkers or therapeutic targets (53). *miR-124a* has also been reported to be related with multiple human diseases. Human chromosome 8q23.1 containing *miR-124a-1* locus is a hotspot. Microdeletions on this locus are associated with psychiatric disorders such as schizophrenia, autism, and social impairment (9–12). Our previous study demonstrated the possibility that a critical role of *miR-124a-1* in prefrontal cortex function contributes to the pathogenesis of those diseases by subjecting *miR-124a-1*$^{+/-}$ mice to a comprehensive behavioral battery (13). As mentioned above, the expression level of *miR-124a* decreases in brain tissues from subjects with FTD (41). This study suggests that *miR-124a* is associated with pathological mechanisms of FTD through regulating Tardbp by analyzing *miR-124a-1/2* DKO mice. Furthermore, the previous studies reported that

Table 1. The expression level of *miR-124a* in human diseases.

Human diseases	The expression level of *miR-124a*	References
Frontotemporal dementia (FTD)	Decreases in brains	41
Alzheimer's disease	Decreases in brains	54, 55
Alzheimer's disease	Increases in brains	56
Acute ischemic stroke	Increases in serum exosomes	57
Atrial fibrillation	Increases in plasma exosomes	58

the expression level of *miR-124a* decreases in human brains with Alzheimer's disease (54, 55), although the other previous study reported that the expression level of *miR-124a* increases in human brains with Alzheimer's disease (56). The expression level of serum exosomal *miR-124a* was significantly higher in acute ischemic stroke patients (57). Also, *miR-124a* was upregulated in plasma exosomes extracted from patients with atrial fibrillation (58). These previous studies suggest the potential of *miR-124a* as a biomarker in various human diseases (Table 1); however, how *miR-124a* is involved in those human diseases remains unclear. Our results would be informative to elucidate the roles of *miR-124a* in those human diseases in the future.

Taken together, the current results indicate that neuronal miRNA, *miR-124a* plays a crucial role in neuronal maturation rather than neurogenesis and may be associated with pathological mechanisms of neurodegenerative diseases such as ALS and FTD through regulating Tardbp (Fig. 18).

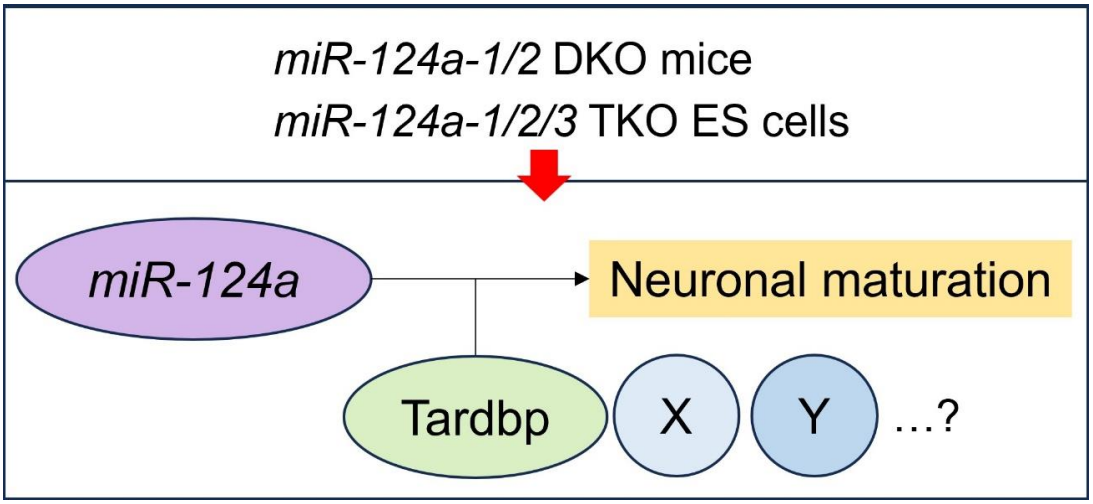

Figure 18. Model of *miR-124a* function *in vivo*.

In this paper, we generated and analyzed *miR-124a-1/2* DKO mice and *miR-124a* TKO ES cells. The current study suggest that *miR-124a* plays a crucial role in neuronal maturation rather than neurogenesis and is associated with pathological mechanisms of neurodegenerative diseases including ALS and FTD by regulating Tardbp.

Material and Methods

Animal care

All procedures were approved by the Institutional Safety Committee on Recombinant DNA Experiments (approval ID 04220-4) and Animal Experimental Committees of the Institute for Protein Research at Osaka University (approval ID 29-01-4). These procedures were performed in compliance with the institutional guidelines. Mice were housed in a temperature-controlled room at 22 °C with a 12 h light/dark cycle. Fresh water and rodent diet were available at all times.

Generation of *miR-124a-1, -2,* and *-3* mutant mice

We obtained *miR-124a-2* and *-3* genomic clones from a screening of the *129S6/SvEvTac* mouse genomic DNA library. We obtained ~6.1-kb and ~5.1-kb fragments for *miR-124a-2*, and ~8.2-kb and ~5.7-kb fragments for *miR-124a-3* from the genomic clones. We subcloned them into a modified pPNT vector (59). We transfected the linearized targeting construct into a *129S6/SvEvTac*-derived TC1 ES cell line (59). The culture, electroporation, and selection of ES cells were performed as previously described (60). ES cell colonies that were resistant to G418 were analyzed by Southern blotting for homologous recombination events. ES cells that were heterozygous for the targeted gene disruption were microinjected into C57BL/6 blastocysts to obtain chimeric mice. We mated this mouse line with a *CAG-Cre* transgenic *129S6/SvEvTac* mouse line (61), which expresses Cre recombinase under the control of the CAG promoter, to obtain null alleles of *miR-124a-2* and *miR-124a-3*. We used *miR-124a-1* (8), *-2*, and *-3 129S6/SvEvTac* mice to generate multiple *miR-124a* mutant mice.

Generation of *miR-124a* TKO ES cell

To target all three *miR-124a* precursors simultaneously, pX330 plasmids (62) expressing both the mammalian-codon-optimized Cas9 and guide RNAs (gRNAs), which target *miR-124a-1/2/3* loci, were transfected into mouse ES cells by electroporation using GENE Pulser II (Bio-Rad). A plasmid containing *PGK-neo* cassette was co-transfected into cells. Neomycin-resistant cells were selected by culturing in G418-containing medium. To identify clones with biallelic mutations in all three genes, the PCR products of *miR-124a-1/2/3* precursor regions from the genomic DNA of these ES lines were sequenced. The primer sequences for the gRNA expression plasmid are shown in Table 2.

Plasmid construction

Plasmids expressing EGFP and FLAG-tagged EGFP were previously constructed (63, 64). Full-length cDNA fragment of mouse *Tardbp* was amplified by PCR using mouse retinal cDNA as a template and subcloned into the pCAGGSII-3xFLAG vector (65). For *Tardbp* knockdown, the Tardbp-shRNA and shRNA-control cassette was subcloned into pBAsi-mU6 vector (Takara). The target sequences were as follows: Tardbp-shRNA1, 5'-GGTGTTGCTGTCCACAGTTAC-3'; Tardbp-shRNA2, 5'-GCGATGGTGTGACTGTAAACT-3'; Tardbp-shRNA3, 5'-GCATGCAGAGGGAACCAAATC-3'; shRNA-control, 5'-GACGTCTAACGGATTCGAGCT-3' (66). Primer sequences used for amplification are shown in Table 2.

PAGE northern blot analysis

The PAGE northern blot analysis was performed as described previously (8). Briefly, total RNAs from mouse tissues were isolated by Trizol (Invitrogen), and 20 μg of the total RNAs were denatured in 5 mM EDTA containing formamide at 80 °C for 5 min. RNAs were separated on 15 % denaturing (7 M urea) polyacrylamide gels. RNAs were transferred to a nylon membrane (Pall Corporation Biodyne). LNA-modified anti–*miR-124a* (Exiqon, 20 pmol) was end-labeled with γ-32P-ATP (Muromachi Yakuhin) using T4 polynucleotide kinase (Takara). The nylon filters were hybridized with the labeled probe in salmon sperm–containing hybridization solution (120 mM sodium phosphate (pH 7.2), 250 mM sodium chloride, 7 % SDS, and 50 % formamide) at 43 °C overnight. The filters were exposed to X-ray film.

Cell culture and transfection

HEK293T and Neuro2a cells were cultured in DMEM (Sigma) containing 10% fetal bovine serum (FBS) supplemented with penicillin (100 μg/ml) and streptomycin (100 μg/ml) at 37 °C with 5% CO_2. Transfection was performed with the calcium phosphate method for HEK293T cells or Lipofectamine 3000 (Thermo Fisher Scientific) for Neuro2a cells.

Western blot analysis

Western blot analysis was performed as previously described (67). Briefly, HEK293T cells were washed with Tris-buffered saline (TBS) twice and lysed in a SDS-sample buffer. The samples were resolved by SDS-PAGE and transferred to PVDF membrane using the iBlot system (Invitrogen). The membranes were blocked with blocking buffer (3% skim milk, and 0.05% Tween 20 in TBS) and incubated with primary antibodies overnight at

4°C. The membranes were washed with 0.05% Tween 20 in TBS three times for 10 min each and then incubated with secondary antibodies for 2 h at room temperature. Signals were detected using Chemi-Lumi One L (Nakalai Tesque). We used the following primary antibodies: mouse anti-FLAG M2 (1:10,000, Sigma, F1804) and rabbit anti-GFP (1:2,500, MBL, 598). The following secondary antibodies were used: horseradish peroxidase-conjugated anti-mouse IgG (1:10,000, Zymed) and anti-rabbit IgG (1:10,000, Jackson Laboratory).

Cell differentiation induction

Differentiation of Neuro2a cells was performed as previously described (68). After 24 h of transfection, the medium was changed to DMEM with 2% FBS containing 20 μM retinoic acid and cultured for 48 h.

Immunofluorescent staining of brain sections and cells

Immunohistochemistry and immunocytochemistry were performed as previously described (69) with certain modifications. For immunohistochemistry, 30-μm brain sections were washed twice in phosphate-buffered saline (PBS), permeabilized with 0.1 % Triton X-100 in PBS, and then incubated with PBS containing 4 % donkey serum for 1 h for blocking. The samples were incubated with a primary antibody at 4 °C overnight. After PBS-washing, these samples were incubated with fluorescent-labeled secondary antibodies at room temperature for 2 h. For immunocytochemistry, cells were fixed with 4 % paraformaldehyde (PFA) in PBS for 5 or 15 min, washed once or twice with PBS, and then incubated in 4 % normal donkey serum and 0.05% Triton X-100 in PBS or 5 % normal donkey serum and 0.1% Triton X-100 in PBS for blocking. The

samples were incubated with a primary antibody at 4 °C overnight. After PBS-washing, these samples were incubated with fluorescent-labeled secondary antibodies at room temperature for 2 h. The specimens were observed under a laser confocal microscope (LSM700, Carl Zeiss). Hoechst (Sigma) or DAPI (Nacalai Tesque) was used for nuclear staining. The primary antibodies were as follows: rabbit anti-CALB1 (Sigma, PC253L, 1:1000), mouse anti-Tuj1 (Covance, MMS-435P, 1:500), rabbit anti-FLAG (1:1,000, Sigma, F7425), and mouse anti-α-tubulin (Sigma, DM1A, 1:1,000, T9026) antibodies. We used Cy3-conjugated (Jackson ImmunoResearch Laboratories, 1:500) and Alexa Fluor 488-conjugated (Sigma, 1:500) secondary antibodies.

Nissl staining

Nissl staining was performed as previously described (63). Coronal sections (30 μm thick) from frozen mouse brains at 2M were stained with 0.1% cresyl violet for 5 min, washed in 100 % ethanol, and incubated in xylene. Slides were coverslipped with Permount (Fisher Scientific).

Induction of neuronal differentiation from ES cells

ES cells were maintained using mouse primary embryonic fibroblasts (30). We used ES cell culture medium containing Knockout DMEM/F12 (Gibco) supplemented with 20 % knockout serum replacement (KSR, Gibco), penicillin/streptomycin, 2-mercaptoethanol, L-glutamine, non-essential amino acids (Sigma), 10 μM MEK inhibitor (PD 0325901, Cayman Chemical Company), 10 μM GSK3 inhibitor (CHIR99021, Cayman Chemical Company), and 10 ng/mL leukemia inhibitory factor. The procedure of differentiation of ES cells into neurons was described previously (30, 31). In brief, ES cells were suspended

in CDM medium containing Iscove's modified Dulbecco's medium/Hams F12 1:1 (Gibco), 1 × lipid concentrate (Gibco), penicillin/streptomycin, transferrin (150 μg/mL final, Sigma), insulin (7 μg/mL, Sigma), 450 μM monothioglycerol (Sigma), and plated onto a 10-cm Lipidure coated dish (Sumitomo Bakelite). After 8 days, aggregated cells were dissociated using 25% Accumax (Innovate Cell Technologies) in PBS, plated onto a 10-cm dish coated with laminin and poly-L-lysine using N2/B27 medium containing 0.5 % N-2 Supplement (Gibco) and 1 % B-27 Supplement (Gibco) in DMEM/F12, and cultured for 12 to 13 days.

RNA-seq and data analysis

RNA-seq analysis was performed as previously described (70), with certain modifications. Total RNAs from the control and *miR-124a-1/2* DKO mouse brains at E17.5 were isolated using TRIzol RNA extraction reagent (Invitrogen). Sequencing was performed on an Illumina NovaSeq 6000 platform in the 101-base single-end mode. The raw reads were mapped to the mouse reference genome sequences (mm10) using the software TopHat ver. 2.0.13, in combination with Bowtie2 ver. 2.3.5.1 and SAMtools ver. 1.11. The numbers of reads were 10,275,949 for Control-1, 11,664,879 for Control-2, 11,416,851 for Control-3, 10,954,843 for CKO-1, 13,526,133 for CKO-2, and 12,471,336 for CKO-3. The number of fragments per kilobase of exon per million mapped fragments (FPKMs) was calculated using Cufflinks ver. 2.2.1. Using the cut-off (fold change > 1.2, < −1.2; $p < 0.05$, unpaired t-test), we obtained 223 down-regulated and 395 up-regulated genes in the *miR-124a-1/2* DKO mouse brain. Heatmap visualization was conducted using the web tool ClustVis (71) under default parameters with FPKM values. Pathway analyses were performed using Integrated Differential Expression and Pathway Analysis (iDEP) v. 0.93

(72) under default parameters with the raw counts, and miRTarBase and GO Biological Process were selected as gene sets. Upstream regulator analysis was carried out using IPA (Qiagen) with FPKM values. IPA was applied to predict the activated or inhibited transcription factors based on the observed differential gene expression profiles. Statistical thresholds were determined through the calculation of the activation z score of gene sets composed of randomly chosen perturbed genes with random sign of fold change that do not lead to significant results on average (Ingenuity Downstream Effects Analysis, whitepaper). Adjusted p values (adj. Pval) and activated z-scores were used to identify significant pathways and upstream regulators. The adj. P val indicates significance, while z-scores were used to define activation (z-score ≥ 2.0) or inhibition (z-score ≤ -2.0). The strongest predicted activation corresponds to z scores ≥ 2, and the strongest predicted inhibition corresponds to z scores ≤ -2.

qRT-PCR

qRT-PCR was performed as described previously (73). Total RNA was extracted using Trizol reagent (Invitrogen), and reverse transcribed into cDNA using SuperScript II reverse transcriptase (Invitrogen) with random hexamers and Oligo dT (Invitrogen). Quantitative PCR was performed using a SYBR GreenER qPCR SuperMix Universal (Invitrogen) and Thermal Cycler Dice Real Time System Single MRQ TP870 (Takara) in accordance with the manufacturer's instructions. Quantification was carried out by Thermal Cycler Dice Real Time System software version 2.0 (Takara). Nucleotide sequences of primers are shown in Table 2 (74, 75).

Statistical analysis

Statistical analyses were performed using GraphPad Prism version 6.04 (GraphPad Software). Single comparisons were performed with an unpaired t-test, while multiple comparisons were performed using one-way analysis of variance (ANOVA) with *post hoc* Tukey–Kramer test. The statistical significance of experiments involving three or more groups and two or more treatments was assessed by two-way ANOVA with *post hoc* Bonferroni test. Data are reported as the median (center line), ±1.5 interquartile range (box), minimal and maximal values (whiskers) or as the mean ± SD. The analyzed number of samples is indicated in the figure legends. Asterisks indicate significance values as follows: $*p < 0.05$, $**p < 0.01$, $***p < 0.001$, and $****p < 0.0001$.

Data availability

All sequencing data is available on GEO (GSE196356).

Table 2. Sequences of DNA oligonucleotides.

Southern blotting probe	Sequence (5' to 3')	Reference
miR-124a-2 5probe 51	GAAGTTGCACCTCTCCAGTGTTCCAGTG	
miR-124a-2 5probe 31	GTCACACTGATAACATCCCTCAGTGCTC	
miR-124a-2 3probe 51	GCTTCTACCCTGAAGACATAGACATG	
miR-124a-2 3probe 31	AGCAGAAGTAGAAATCGGCTTCTCTCAG	
miR-124a-3 5probe 51	ATTTCTGCCCCGCTCGAGAGCACAGCTC	
miR-124a-3 5probe 31	GCAGTGAGGAAGGATGGCTTGGGCCATG	
miR-124a-3 3probe 51	CGATGTTGTCCACGACTCCGTACAGGCA	
miR-124a-3 3probe 31	GCTCACAGCTGTCTATGGGCAAGCTGTC	
qPCR primer		
NeuroD1-F	TCCAGGGTTATGAGATCGTCA	
NeuroD1-R	TCGCTGTATGATTTGGTCATG	
GAD2-F	GTGGAAGCTGAGTGGAGTAGAGAG	
GAD2-R	GTCTCCTGTGTCATAGGACAGGTC	
Vglut1-F	TGCCAGCATCTTGATGGGCATTTC	
Vglut1-R	CTATGAGGAACACGTACTGCCAC	
Gfap-F	GTTAAGCTAGCCCTGGACATCGAG	
Gfap-R	GATCTGGAGGTTGGAGAAAGTCTG	
Nanog-F	GAACTCTCCTCCATTCTGAACCTG	
Nanog-R	AGACCATTGCTAGTCTTCAACCAC	
Tuj1-F	GACTTGGAACCTGGAACCATGGAC	
Tuj1-R	CAGTTGTTGCCAGCACCACTCTGA	
Map2-F	GACAATGCTCACCACGTACCTGGA	
Map2-R	GATGATCTCAGCCCCGTGATCTAC	
Itgb1-F	AGGTCGATCCTGTGACCCATTGCA	
Itgb1-R	GAACAATTCCAGCAACCACGCCTG	
mTardbp-QPCR-51	GTGTGACTGTAAACTTCCCAACTC	
mTardbp-QPCR-31	TACAACGTCCAACAAACACCTTTC	
mSrebf2-QPCR-51	ATCCTACCAAGCACACTGATTGAG	
mSrebf2-QPCR-31	CAGACTCTGGGCACGATTTAAGAA	
mNupr1-QPCR-51	GAATATGATCAGTACAGCCTGGC	46
mNupr1-QPCR-31	CAGAGTTCTGGAACTTGGTCAGC	46
mKlf6-QPCR-51	ACCCGACATGGATGTGCTCCCAAT	47
mKlf6-QPCR-31	GCAGGGCTCACTCTGAAGATA	47
Rpl4-F	GATATGCCATCTGTTCTGCCCT	
Rpl4-R	CTTGCCAGCTCTCATTCTCTGA	
Construct		
mTardbp-ORF-SalI-51	GGGGTCGACATGTCTGAATATATTCGGGTAACAGAA	
mTardbp-ORF-NotI-31	GGGGCGGCCGCCTACATTCCCCAGCCAGAAGACTTAGA	
CRISPR		
mir124-1-sgRNA-F	GTCGACTAATACGACTCACTATAGGTCCATACAATTAAGGCACG	
mir124-2-sgRNA-F	GTCGACTAATACGACTCACTATAGTGTCATACAATTAAGGCACG	
mir124-3-sgRNA-F	GTCGACTAATACGACTCACTATAGGTCTATACAATTAAGGCACG	
sgRNA-R	GGATCCAAAAGCACCGACTCGGTGCC	
Genotyping		
miR-124a-2-tail-F	TAGGTGCGCTGTAAATGGCATG	
miR-124a-2-tail-R	TGAATCAATGCGAGGGGTCCT	
miR-124a-3-tail-F	GTGATACTCATGACATCCCTTCGT	
miR-124a-3-tail-R	TCTGCGTGTTCACAGCGGACCTTGAT	
pPNT-lox-neo-F	ATATGATCGGAATTGGTCTCCCG	

Acknowledgements

I express my appreciation to Prof. Takahisa Furukawa for his continuous and thoughtful guidance. I am also particularly grateful to Associate Prof. Taro Chaya who gave me kind instruction about research plan, experimental design, and experimental technique. I acknowledge with appreciation the crucial roles of R. Sugimura, D. Okuzaki, S. Watanabe, L. R. Varner, D. Motooka, D. Gyoten, H. Yamamoto, and H. Kato. I thank M. Shimada, T. Kozuka, M. Kadowaki, A. Tani, A. Ishimaru, T. Nakayama, S. Gion, M. Wakabayashi, H. Abe, M. Nakamura, and K. Yoshida for technical assistance. I acknowledge the NGS core facility of the Genome Information Research Center at the Research Institute for Microbial Diseases of Osaka University for their support with RNA sequencing and data analysis.

References

1. Ramanathan, K., Fekadie, M., Padmanabhan, G., and Gulilat, H. (2023) Long noncoding RNA: An emerging diagnostic and therapeutic target in kidney diseases. *Cell Biochem. Funct.* 10.1002/cbf.3901

2. Bartel, D. P. (2004) MicroRNAs: Genomics, Biogenesis, Mechanism, and Function. *Cell*. **116**, 281–297

3. Feinbaum, R., Ambros, V., and Lee, R. (1993) The C. elegans Heterochronic Gene lin-4 Encodes Small RNAs with Antisense Complementarity to lin-14. *Cell*. **116**, 843–854

4. Pasquinelli, A. E., Reinhart, B. J., Slack, F., Martindale, M. Q., Kuroda, M. I., Maller, B., Hayward, D. C., Ball, E. E., Degnan, B., Müller, P., Spring, J., Srinivasan, A., Fishman, M., Finnerty, J., Corbo, J., Levine, M., Leahy, P., Davidson, E., and Ruvkun, G. (2000) Conservation of the sequence and temporal expression of let-7 heterochronic regulatory RNA. *Nature*. **408**, 86–89

5. Kozomara, A., Birgaoanu, M., and Griffiths-Jones, S. (2019) MiRBase: From microRNA sequences to function. *Nucleic Acids Res.* **47**, D155–D162

6. He, L., and Hannon, G. J. (2004) MicroRNAs: Small RNAs with a big role in gene regulation. *Nat. Rev. Genet.* **5**, 522–531

7. Lagos-Quintana, M., Rauhut, R., Yalcin, A., Meyer, J., Lendeckel, W., and Tuschl, T. (2002) Identification of tissue-specific MicroRNAs from mouse. *Curr. Biol.* **12**, 735–739

8. Sanuki, R., Onishi, A., Koike, C., Muramatsu, R., Watanabe, S., Muranishi, Y., Irie, S., Uneo, S., Koyasu, T., Matsui, R., Chérasse, Y., Urade, Y., Watanabe, D., Kondo, M., Yamashita, T., and Furukawa, T. (2011) MiR-124a is required for hippocampal axogenesis and retinal cone survival through Lhx2 suppression. *Nat. Neurosci.* **14**, 1125–1136

9. Longoni, M., Lage, K., Russell, M. K., Loscertales, M., Abdul-Rahman, O. A., Baynam, G., Bleyl, S. B., Brady, P. D., Breckpot, J., Chen, C. P., Devriendt, K., Gillessen-Kaesbach, G., Grix, A. W., Rope, A. F., Shimokawa, O., Strauss, B., Wieczorek, D., Zackai, E. H., Coletti, C. M., Maalouf, F. I., Noonan, K. M., Park, J. H., Tracy, A. A., Lee, C., Donahoe, P. K., and Pober, B. R. (2012) Congenital diaphragmatic hernia interval on chromosome 8p23.1 characterized by genetics and protein interaction networks. *Am. J. Med. Genet. Part A.* **158 A**, 3148–3158

10. Bassett, A. S., Costain, G., Fung, W. L. A., Russell, K. J., Pierce, L., Kapadia, R., Carter, R. F., Chow, E. W. C., and Forsythe, P. J. (2010) Clinically detectable copy number variations in a Canadian catchment population of schizophrenia. *J. Psychiatr. Res.* **44**, 1005–1009

11. Takahashi, S., Faraone, S. V., Lasky-Su, J., and Tsuang, M. T. (2005) Genome-wide scan of homogeneous subtypes of NIMH genetics initiative schizophrenia families. *Psychiatry Res.* **133**, 111–122

12. Devriendt, K., Matthijs, G., Van Dael, R., Gewillig, M., Eyskens, B., Hjalgrim, H., Dolmer, B., McGaughran, J., Bröndum-Nielsen, K., Marynen, P., Fryns, J. P., and Vermeesch, J. R. (1999) Delineation of the critical deletion region for congenital heart defects, on chromosome 8p23.1. *Am. J. Hum. Genet.* **64**, 1119–1126

13. Kozuka, T., Omori, Y., Watanabe, S., Tarusawa, E., Yamamoto, H., Chaya, T., Furuhashi, M., Morita, M., Sato, T., Hirose, S., Ohkawa, Y., Yoshimura, Y., Hikida, T., and Furukawa, T. (2019) miR-124 dosage regulates prefrontal cortex function by dopaminergic modulation. *Sci. Rep.* **9**, 1–14

14. Miska, E. A., Alvarez-Saavedra, E., Abbott, A. L., Lau, N. C., Hellman, A. B., McGonagle, S. M., Bartel, D. P., Ambros, V. R., and Horvitz, H. R. (2007) Most Caenorhabditis elegans microRNAs are individually not essential for development or viability. *PLoS Genet.* **3**, 2395–2403

15. Clark, A. M., Goldstein, L. D., Tevlin, M., Tavaré, S., Shaham, S., and Miska, E. A. (2010) The microRNA miR-124 controls gene expression in the sensory nervous system of Caenorhabditis elegans. *Nucleic Acids Res.* **38**, 3780–3793

16. Weng, R., and Cohen, S. M. (2012) Drosophila miR-124 regulates neuroblast proliferation through its target anachronism. *Development*. **139**, 1427–1434

17. Sun, K., Westholm, J. O., Tsurudome, K., Hagen, J. W., Lu, Y., Kohwi, M., Betel, D., Gao, F. B., Haghighi, A. P., Doe, C. Q., and Lai, E. C. (2012) Neurophysiological defects and neuronal gene deregulation in drosophila mir-124 mutants. *PLoS Genet.* 10.1371/journal.pgen.1002515

18. Visvanathan, J., Lee, S., Lee, B., Lee, J. W., and Lee, S. K. (2007) The microRNA miR-124 antagonizes the anti-neural REST/SCP1 pathway during embryonic CNS development. *Genes Dev.* **21**, 744–749

19. Makeyev, E. V., Zhang, J., Carrasco, M. A., and Maniatis, T. (2007) The MicroRNA miR-124 Promotes Neuronal Differentiation by Triggering Brain-Specific Alternative Pre-mRNA Splicing. *Mol. Cell*. **27**, 435–448

20. Cao, X., Pfaff, S. L., and Gage, F. H. (2007) A functional study of miR-124 in the developing neural tube. *Genes Dev.* **21**, 531–536

21. Yu, J. Y., Chung, K. H., Deo, M., Thompson, R. C., and Turner, D. L. (2008) MicroRNA miR-124 regulates neurite outgrowth during neuronal differentiation. *Exp. Cell Res.* **314**, 2618–2633

22. Franke, K., Otto, W., Johannes, S., Baumgart, J., Nitsch, R., and Schumacher, S. (2012) miR-124-regulated RhoG reduces neuronal process complexity via ELMO/Dock180/Rac1 and Cdc42 signalling. *EMBO J.* **31**, 2908–2921

23. Kutsche, L. K., Gysi, D. M., Fallmann, J., Lenk, K., Petri, R., Swiersy, A., Klapper, S. D., Pircs, K., Khattak, S., Stadler, P. F., Jakobsson, J., Nowick, K., and Busskamp, V. (2018) Combined Experimental and System-Level Analyses Reveal the Complex Regulatory Network of miR-124 during Human Neurogenesis. *Cell Syst.* **7**, 438-452.e8

24. Cheng, L. C., Pastrana, E., Tavazoie, M., and Doetsch, F. (2009) MiR-124 regulates adult neurogenesis in the subventricular zone stem cell niche. *Nat. Neurosci.* **12**, 399–408

25. Kabashi, E., Lin, L., Tradewell, M. L., Dion, P. A., Bercier, V., Bourgouin, P., Rochefort, D., Bel Hadj, S., Durham, H. D., Velde, C. Vande, Rouleau, G. A., and Drapeau, P. (2009) Gain and loss of function of ALS-related mutations of TARDBP (TDP-43) cause motor deficits *in vivo*. *Hum. Mol. Genet.* **19**, 671–683

26. Diaper, D. C., Adachi, Y., Sutcliffe, B., Humphrey, D. M., Elliott, C. J. H., Stepto, A., Ludlow, Z. N., Broeck, L. Vanden, Callaerts, P., Dermaut, B., Al-Chalabi, A., Shaw, C. E., Robinson, I. M., and Hirth, F. (2013) Loss and gain of Drosophila TDP-43 impair synaptic efficacy and motor control leading to age-related neurodegeneration by loss-of-function phenotypes. *Hum. Mol. Genet.* **22**, 1539–1557

27. Kraemer, B. C., Schuck, T., Wheeler, J. M., Robinson, L. C., Trojanowski, J. Q., Lee, V. M. Y., and Schellenberg, G. D. (2010) Loss of Murine TDP-43 disrupts motor function and plays an essential role in embryogenesis. *Acta Neuropathol.* **119**, 409–419

28. Sephton, C. F., Good, S. K., Atkin, S., Dewey, C. M., Mayer, P., Herz, J., and Yu, G. (2010) TDP-43 is a developmentally regulated protein essential for early embryonic development. *J. Biol. Chem.* **285**, 6826–6834

29. Wu, L. S., Cheng, W., Hou, S. C., Yan, Y. T., Jiang, S. T., and Shen, C. K. J. (2010) TDP-43, a neuro-pathosignature factor, is essential for early mouse embryogenesis. *Genesis*. **48**, 56–62

30. Bouhon, I. A., Kato, H., Chandran, S., and Allen, N. D. (2005) Neural differentiation of mouse embryonic stem cells in chemically defined medium. *Brain Res. Bull.* **68**, 62–75

31. Kohama, C., Kato, H., Numata, K., Hirose, M., Takemasa, T., Ogura, A., and Kiyosawa, H. (2012) ES cell differentiation system recapitulates the

establishment of imprinted gene expression in a cell-type-specific manner. *Hum. Mol. Genet.* **21**, 1391–1401

32. Graus-Porta, D., Blaess, S., Senften, M., Littlewood-Evans, A., Damsky, C., Huang, Z., Orban, P., Klein, R., Schittny, J. C., and Müller, U. (2001) β1-Class integrins regulate the development of laminae and folia in the cerebral and cerebellar cortex. *Neuron*. **31**, 367–379

33. Schmid, R. S., and Anton, E. S. (2003) Role of integrins in the development of the cerebral cortex. *Cereb. Cortex*. **13**, 219–224

34. Dulabon, L., Olson, E. C., Taglienti, M. G., Eisenhuth, S., McGrath, B., Walsh, C. A., Kreidberg, J. A., and Anton, E. S. (2000) Reelin binds α3β1 integrin and inhibits neuronal migration. *Neuron*. **27**, 33–44

35. Rajasethupathy, P., Fiumara, F., Sheridan, R., Betel, D., Puthanveettil, S. V., Russo, J. J., Sander, C., Tuschl, T., and Kandel, E. (2009) Characterization of Small RNAs in Aplysia Reveals a Role for miR-124 in Constraining Synaptic Plasticity through CREB. *Neuron*. **63**, 803–817

36. Yang, Y., Shu, X., Liu, D., Shang, Y., Wu, Y., Pei, L., Xu, X., Tian, Q., Zhang, J., Qian, K., Wang, Y. X., Petralia, R. S., Tu, W., Zhu, L. Q., Wang, J. Z., and Lu, Y. (2012) EPAC Null Mutation Impairs Learning and Social Interactions via Aberrant Regulation of miR-124 and Zif268 Translation. *Neuron*. **73**, 774–788

37. Hou, Q., Ruan, H., Gilbert, J., Wang, G., Ma, Q., Yao, W. D., and Man, H. Y. (2015) MicroRNA miR124 is required for the expression of homeostatic synaptic plasticity. *Nat. Commun.* **6**, 1–12

38. Iguchi, Y., Katsuno, M., Niwa, J. I., Takagi, S., Ishigaki, S., Ikenaka, K., Kawai, K., Watanabe, H., Yamanaka, K., Takahashi, R., Misawa, H., Sasaki, S., Tanaka, F., and Sobue, G. (2013) Loss of TDP-43 causes age-dependent progressive motor neuron degeneration. *Brain*. **136**, 1371–1382

39. Ma, X. R., Prudencio, M., Koike, Y., Vatsavayai, S. C., Kim, G., Harbinski, F., Briner, A., Rodriguez, C. M., Guo, C., Akiyama, T., Schmidt, H. B., Cummings,

B. B., Wyatt, D. W., Kurylo, K., Miller, G., Mekhoubad, S., Sallee, N., Mekonnen, G., Ganser, L., Rubien, J. D., Jansen-West, K., Cook, C. N., Pickles, S., Oskarsson, B., Graff-Radford, N. R., Boeve, B. F., Knopman, D. S., Petersen, R. C., Dickson, D. W., Shorter, J., Myong, S., Green, E. M., Seeley, W. W., Petrucelli, L., and Gitler, A. D. (2022) TDP-43 represses cryptic exon inclusion in the FTD–ALS gene UNC13A. *Nature*. **603**, 124–130

40. Brown, A. L., Wilkins, O. G., Keuss, M. J., Hill, S. E., Zanovello, M., Lee, W. C., Bampton, A., Lee, F. C. Y., Masino, L., Qi, Y. A., Bryce-Smith, S., Gatt, A., Hallegger, M., Fagegaltier, D., Phatnani, H., Phatnani, H., Kwan, J., Sareen, D., Broach, J. R., Simmons, Z., Arcila-Londono, X., Lee, E. B., Van Deerlin, V. M., Shneider, N. A., Fraenkel, E., Ostrow, L. W., Baas, F., Zaitlen, N., Berry, J. D., Malaspina, A., Fratta, P., Cox, G. A., Thompson, L. M., Finkbeiner, S., Dardiotis, E., Miller, T. M., Chandran, S., Pal, S., Hornstein, E., MacGowan, D. J., Heiman-Patterson, T., Hammell, M. G., Patsopoulos, N. A., Butovsky, O., Dubnau, J., Nath, A., Bowser, R., Harms, M., Aronica, E., Poss, M., Phillips-Cremins, J., Crary, J., Atassi, N., Lange, D. J., Adams, D. J., Stefanis, L., Gotkine, M., Baloh, R. H., Babu, S., Raj, T., Paganoni, S., Shalem, O., Smith, C., Zhang, B., Harris, B., Broce, I., Drory, V., Ravits, J., McMillan, C., Menon, V., Wu, L., Altschuler, S., Lerner, Y., Sattler, R., Van Keuren-Jensen, K., Rozenblatt-Rosen, O., Lindblad-Toh, K., Nicholson, K., Gregersen, P., Lee, J. H., Kokos, S., Muljo, S., Newcombe, J., Gustavsson, E. K., Seddighi, S., Reyes, J. F., Coon, S. L., Ramos, D., Schiavo, G., Fisher, E. M. C., Raj, T., Secrier, M., Lashley, T., Ule, J., Buratti, E., Humphrey, J., Ward, M. E., and Fratta, P. (2022) TDP-43 loss and ALS-risk SNPs drive mis-splicing and depletion of UNC13A. *Nature*. **603**, 131–137

41. Gascon, E., Lynch, K., Ruan, H., Almeida, S., Verheyden, J. M., Seeley, W. W., Dickson, D. W., Petrucelli, L., Sun, D., Jiao, J., Zhou, H., Jakovcevski, M., Akbarian, S., Yao, W. D., and Gao, F. B. (2014) Alterations in microRNA-124 and AMPA receptors contribute to social behavioral deficits in frontotemporal dementia. *Nat. Med.* **20**, 1444–1451

42. Sempere, L. F., Freemantle, S., Pitha-Rowe, I., Moss, E., Dmitrovsky, E., and Ambros, V. (2004) Expression profiling of mammalian microRNAs uncovers a

subset of brain-expressed microRNAs with possible roles in murine and human neuronal differentiation. *Genome Biol.* 10.1186/gb-2004-5-3-r13

43. Krichevsky, A. M., King, K. S., Donahue, C. P., Khrapko, K., and Kosik, K. S. (2004) Erratum: A microRNA array reveals extensive regulation of microRNAs during brain development (RNA (2003) 9 (1274-1281)). *Rna*. **10**, 551

44. Yoo, A. S., Staahl, B. T., Chen, L., and Crabtree, G. R. (2009) MicroRNA-mediated switching of chromatin-remodelling complexes in neural development. *Nature*. **460**, 642–646

45. Huang, T., Liu, Y., Huang, M., Zhao, X., and Cheng, L. (2010) Wnt1-cre-mediated conditional loss of Dicer results in malformation of the midbrain and cerebellum and failure of neural crest and dopaminergic differentiation in mice. *J. Mol. Cell Biol.* **2**, 152–163

46. Calin, G. A., and Croce, C. M. (2006) MicroRNA signatures in human cancers. *Nat. Rev. Cancer*. **6**, 857–866

47. Sayed, D., Hong, C., Chen, I. Y., Lypowy, J., and Abdellatif, M. (2007) MicroRNAs play an essential role in the development of cardiac hypertrophy. *Circ. Res.* **100**, 416–424

48. Carè, A., Catalucci, D., Felicetti, F., Bonci, D., Addario, A., Gallo, P., Bang, M. L., Segnalini, P., Gu, Y., Dalton, N. D., Elia, L., Latronico, M. V. G., Høydal, M., Autore, C., Russo, M. A., Dorn, G. W., Ellingsen, Ø., Ruiz-Lozano, P., Peterson, K. L., Croce, C. M., Peschle, C., and Condorelli, G. (2007) MicroRNA-133 controls cardiac hypertrophy. *Nat. Med.* **13**, 613–618

49. Giraldez, A. J., Cinalli, R. M., Glasner, M. E., Enright, A. J., Thomson, J. M., Baskerville, S., Hammond, S. M., Bartel, D. P., and Schier, A. F. (2005) MicroRNAs regulate brain morphogenesis in zebrafish. *Science (80-.).* **308**, 833–838

50. Chmielarz, P., Konovalova, J., Najam, S. S., Alter, H., Piepponen, T. P., Erfle, H., Sonntag, K. C., Schütz, G., Vinnikov, I. A., and Domanskyi, A. (2017) Dicer

and microRNAs protect adult dopamine neurons. *Cell Death Dis.* 10.1038/CDDIS.2017.214

51. Jopling, C. L., Yi, M. K., Lancaster, A. M., Lemon, S. M., and Sarnow, P. (2005) Molecular biology: Modulation of hepatitis C virus RNA abundance by a liver-specific MicroRNA. *Science (80-.).* **309**, 1577–1581

52. McDonald, J. T., Enguita, F. J., Taylor, D., Griffin, R. J., Priebe, W., Emmett, M. R., Sajadi, M. M., Harris, A. D., Clement, J., Dybas, J. M., Aykin-Burns, N., Guarnieri, J. W., Singh, L. N., Grabham, P., Baylin, S. B., Yousey, A., Pearson, A. N., Corry, P. M., Saravia-Butler, A., Aunins, T. R., Sharma, S., Nagpal, P., Meydan, C., Foox, J., Mozsary, C., Cerqueira, B., Zaksas, V., Singh, U., Wurtele, E. S., Costes, S. V., Davanzo, G. G., Galeano, D., Paccanaro, A., Meinig, S. L., Hagan, R. S., Bowman, N. M., Wallet, S. M., Maile, R., Wolfgang, M. C., Mock, J. R., Torres-Castillo, J. L., Love, M. K., Lovell, W., Rice, C., Mitchem, O., Burgess, D., Suggs, J., Jacobs, J., Altinok, S., Sapoval, N., Treangen, T. J., Moraes-Vieira, P. M., Vanderburg, C., Wallace, D. C., Schisler, J. C., Mason, C. E., Chatterjee, A., Meller, R., and Beheshti, A. (2021) Role of miR-2392 in driving SARS-CoV-2 infection. *Cell Rep.* 10.1016/j.celrep.2021.109839

53. Nemeth, K., Bayraktar, R., Ferracin, M., and Calin, G. A. (2023) Non-coding RNAs in disease: from mechanisms to therapeutics. *Nat. Rev. Genet.* 10.1038/s41576-023-00662-1

54. Smith, P., Al Hashimi, A., Girard, J., Delay, C., and Hébert, S. S. (2011) *In vivo* regulation of amyloid precursor protein neuronal splicing by microRNAs. *J. Neurochem.* **116**, 240–247

55. An, F., Gong, G., Wang, Y., Bian, M., Yu, L., and Wei, C. (2018) Correction: MiR-124 acts as a target for Alzheimer's disease by regulating BACE1 [Oncotarget., 8, (2017) (114065-114071)] DOI:10.18632/oncotarget.23119. *Oncotarget*. **9**, 24871

56. Wang, X., Liu, D., Huang, H. Z., Wang, Z. H., Hou, T. Y., Yang, X., Pang, P., Wei, N., Zhou, Y. F., Dupras, M. J., Calon, F., Wang, Y. T., Man, H. Y., Chen, J. G., Wang, J. Z., Hébert, S. S., Lu, Y., and Zhu, L. Q. (2018) A Novel

MicroRNA-124/PTPN1 Signal Pathway Mediates Synaptic and Memory Deficits in Alzheimer's Disease. *Biol. Psychiatry*. **83**, 395–405

57. Ji, Q., Ji, Y., Peng, J., Zhou, X., Chen, X., Zhao, H., Xu, T., Chen, L., and Xu, Y. (2016) Increased brain-specific MiR-9 and MiR-124 in the serum exosomes of acute ischemic stroke patients. *PLoS One*. **11**, 1–14

58. Zhu, P., Li, H., Zhang, A., Li, Z., Zhang, Y., Ren, M., Zhang, Y., and Hou, Y. (2022) MicroRNAs sequencing of plasma exosomes derived from patients with atrial fibrillation: miR-124-3p promotes cardiac fibroblast activation and proliferation by regulating AXIN1. *J. Physiol. Biochem.* **78**, 85–98

59. Deng, C., Wynshaw-Boris, A., Zhou, F., Kuo, A., and Leder, P. (1996) Fibroblast growth factor receptor 3 is a negative regulator of bone growth. *Cell*. **84**, 911–921

60. Muranishi, Y., Terada, K., Inoue, T., Katoh, K., Tsujii, T., Sanuki, R., Kurokawa, D., Aizawa, S., Tamaki, Y., and Furukawa, T. (2011) An essential role for RAX homeoprotein and NOTCH-HES signaling in Otx2 expression in embryonic retinal photoreceptor cell fate determination. *J. Neurosci.* **31**, 16792–16807

61. Sakai, K., and Miyazaki, J. I. (1997) A transgenic mouse line that retains Cre recombinase activity in mature oocytes irrespective of the cre transgene transmission. *Biochem. Biophys. Res. Commun.* **237**, 318–324

62. Cong, L., Ran, F. A., Cox, D., Lin, S., Barretto, R., Habib, N., Hsu, P. D., Wu, X., Jiang, W., Marraffini, L. A., and Zhang, F. (2013) Multiplex genome engineering using CRISPR/Cas systems. *Science (80-.).* **339**, 819–823

63. Chaya, T., Omori, Y., Kuwahara, R., and Furukawa, T. (2014) ICK is essential for cell type-specific ciliogenesis and the regulation of ciliary transport. *EMBO J.* **33**, 1227–1242

64. Omori, Y., Chaya, T., Katoh, K., Kajimura, N., Sato, S., Muraoka, K., Ueno, S., Koyasu, T., Kondo, M., and Furukawa, T. (2010) Negative regulation of ciliary

length by ciliary male germ cell-associated kinase (Mak) is required for retinal photoreceptor survival. *Proc. Natl. Acad. Sci. U. S. A.* **107**, 22671–22676

65. Irie, S., Sanuki, R., Muranishi, Y., Kato, K., Chaya, T., and Furukawa, T. (2015) Rax Homeoprotein Regulates Photoreceptor Cell Maturation and Survival in Association with Crx in the Postnatal Mouse Retina. *Mol. Cell. Biol.* **35**, 2583–2596

66. Itoh, Y., Moriyama, Y., Hasegawa, T., Endo, T. A., Toyoda, T., and Gotoh, Y. (2013) Scratch regulates neuronal migration onset via an epithelial-mesenchymal transition-like mechanism. *Nat. Neurosci.* **16**, 416–425

67. Tsutsumi, R., Chaya, T., Tsujii, T., and Furukawa, T. (2022) The carboxyl-terminal region of SDCCAG8 comprises a functional module essential for cilia formation as well as organ development and homeostasis. *J. Biol. Chem.* **298**, 101686

68. Sugiyama, T., Yamamoto, H., Kon, T., Chaya, T., Omori, Y., Suzuki, Y., Abe, K., Watanabe, D., and Furukawa, T. (2020) The potential role of Arhgef33 RhoGEF in foveal development in the zebra finch retina. *Sci. Rep.* **10**, 1–11

69. Omori, Y., Chaya, T., Yoshida, S., Irie, S., Tsujii, T., and Furukawa, T. (2015) Identification of G Protein-Coupled Receptors (GPCRs) in primary cilia and their possible involvement in body weight control. *PLoS One*. **10**, 1–17

70. Chaya, T., Ishikane, H., Varner, L. R., Sugita, Y., Maeda, Y., Tsutsumi, R., Motooka, D., Okuzaki, D., and Furukawa, T. (2022) Deficiency of the neurodevelopmental disorder-associated gene Cyfip2 alters the retinal ganglion cell properties and visual acuity. *Hum. Mol. Genet.* **31**, 535–547

71. Metsalu, T., and Vilo, J. (2015) ClustVis: A web tool for visualizing clustering of multivariate data using Principal Component Analysis and heatmap. *Nucleic Acids Res.* **43**, W566–W570

72. Ge, S. X., Son, E. W., and Yao, R. (2018) iDEP: An integrated web application for differential expression and pathway analysis of RNA-Seq data. *BMC Bioinformatics*. **19**, 1–24

73. Chaya, T., Tsutsumi, R., Varner, L. R., Maeda, Y., Yoshida, S., and Furukawa, T. (2019) Cul3-Klhl18 ubiquitin ligase modulates rod transducin translocation during light-dark adaptation. *EMBO J.* **38**, 1–22

74. Liu, J., Song, X., Kuang, F., Zhang, Q., Xie, Y., Kang, R., Kroemer, G., and Tang, D. (2021) NUPR1 is a critical repressor of ferroptosis. *Nat. Commun.* 10.1038/s41467-021-20904-2

75. Matsumoto, N., Kubo, A., Liu, H., Akita, K., Laub, F., Ramirez, F., Keller, G., and Friedman, S. L. (2006) Developmental regulation of yolk sac hematopoiesis by Krüppel-like factor 6. *Blood*. **107**, 1357–1365